Recycling of cell surface membrane proteins from yeast endosomes is regulated by ubiquitinated Ist1

Kamilla ME. Laidlaw[1], Grant Calder[2], Chris MacDonald[1*]

[1] *York Biomedical Research Institute and Department of Biology, University of York, York, UK*
[2] *Imaging and Cytometry Laboratory, Bioscience Technology Facility, Department of Biology, University of York, UK*
[*] *Correspondence: Email: chris.macdonald@york.ac.uk Tel: +44 (0) 1904 328 609*

ABSTRACT

Trafficking of cell surface membrane proteins to and from the plasma membrane impinges on myriad biological processes and ensures correct cellular function. Upon internalization, many surface proteins are recycled back to the plasma membrane. Although these endosomal trafficking pathways control surface protein activity, the precise regulatory features and division of labour between interconnected pathways is poorly defined. Furthermore, how well endosomal trafficking mechanisms are conserved is unclear. In yeast, we show cargo recycling back to the surface occurs through distinct pathways. In addition to retrograde recycling pathways via the late Golgi, used by synaptobrevins and driven by cargo ubiquitination, we find nutrient transporter recycling bypasses the Golgi in a pathway driven by cargo deubiquitination. Nutrient transporters rapidly internalize to, and recycle from, endosomes marked by Vps4 and the ESCRT-III associated factor Ist1. This compartment serves as both 'early' and 'recycling' endosome, implying these features are evolutionarily conserved. Ist1 has previously been implicated in recycling in yeast and other eukaryotes. We show Ist1 is ubiquitinated and this is required for proper endosomal recruitment and cargo recycling to the surface. Additionally, the ubiquitin-binding adaptor Npl4 and the essential ATPase Cdc48 are required for cargo recycling possibly through regulation of ubiquitinated Ist1. This collectively suggests mechanistic features of recycling from endosomes to the plasma membrane are also conserved.

INTRODUCTION

The plasma membrane (PM) of eukaryotic cells hosts a variety of functionally diverse proteins that play critical cellular roles, often detecting extracellular signals and ensuring appropriate responses to the environment. As such, surface membrane proteins represent by far the largest class of molecular therapeutic targets (Santos et al., 2017). Surface proteins are regulated by intracellular transport pathways, relying on different vesicle trafficking steps transiting the secretory pathway to the PM (Stalder and Gershlick, 2020) or endocytic regulation following their initial localization at the surface (Sigismund et al., 2021). Many of these mechanisms are evolutionarily conserved, with fundamental modes of regulation uncovered and explained in the budding yeast *Saccharomyces cerevisiae*.

Surface proteins can be downregulated through endocytosis and trafficking to the lysosome (vacuole in yeast), including the specific downregulation of receptors and transporters recognising ligands and substrates, respectively (Davis et al., 1993; Séron et al., 1999). More general cargo endocytosis can occur *en masse*, such as yeast cells triggering large scale downregulation of surface cargoes in response to nutrient stress (Müller et al., 2015; Laidlaw et al., 2020). Endocytosed surface cargoes that retain a ubiquitination signal are targeted through the multivesicular body (MVB) pathway, packaged into intraluminal vesicles (ILVs), and then delivered to the vacuole for degradation (Urbanowski and Piper, 2001; Katzmann et al., 2001). Ubiquitinated cargoes are recognised by the Endosomal Sorting Complex Required for Transport (ESCRT) complexes, with ESCRT-0 and ESCRT-I abundant in ubiquitin binding domains (Shields et al., 2009). ESCRT-III subunits are recruited to the endosomal/MVB membrane, where they polymerise and drive formation of vesicles budding into the endosome lumen (Hanson et al., 2008; Saksena et al., 2009; Wollert et al., 2009). Filaments created through polymerisation of Snf7, modulated by other ESCRTs and the Vps4 ATPase, drive membrane deformation (Shestakova et al., 2010; Adell et al., 2017; Maity et al., 2019; Tang et al., 2015; Pfitzner et al., 2020). Nutrient transporters in yeast are useful reporters for endosomal trafficking, such as the amino acid transporters Mup1 and Fur4, as their ubiquitination and ESCRT-dependent trafficking to the vacuole can be triggered by addition of substrate (Hein et al., 1995; Keener and Babst, 2013; Isnard et al., 1996). The E3-ligase Rsp5 and its substrate specific adaptors is largely responsible for cargo ubiquitination and vacuolar sorting events (MacDonald et al., 2020; Sardana and Emr, 2021).

Surface activity of internalized PM proteins is also regulated by recycling routes back to the PM (MacDonald and Piper, 2016). Recycling in yeast appears less complex than mammalian cells but the division of labour between certain pathways, and even organisation of the endosomal system, is not fully understood (Day et al., 2018; Laidlaw and MacDonald, 2018; Ma and Burd, 2019). Retrograde recycling of yeast synaptobrevin orthologues, Snc1 and Snc2 (Protopopov et al., 1993), via the *trans*-Golgi network (TGN) has been extensively studied. Localization of Snc1 is polarised with concentration to the bud-tips of emerging daughter cells and the shmoo protrusions induced upon response to mating factor; this polarisation relies on post-endocytic recycling (Valdez-Taubas and Pelham, 2003). Snc1 recycles via the TGN through multiple pathways involving different machinery, such as retromer, Snx4-Atg20 (Lewis et al., 2000; Hettema et al., 2003; Ma et al., 2017) and other factors, including phospholipid flippases, Rcy1, and Ypt31/32 (Galan et al., 2001; Hua et al., 2002; Chen et al., 2005; Furuta et al., 2007; Hanamatsu et al., 2014). Retrograde recycling of Snc1 also requires its ubiquitination to facilitate interaction with endosomally localized COPI (Xu et al., 2017). This is an intriguing observation, as ubiquitinated Snc1 can be incorporated into the MVB pathway and sort to the vacuole during stress conditions (Chen et al., 2014; MacDonald et al., 2015). However, this suggests that under normal conditions the primary role of Snc1 ubiquitination is for recycling and implies different ubiquitin-receptors dedicated to distinct pathways operate, even within the yeast endosomal network.

Unlike Snc1, deubiquitination of other cargoes, like nutrient transporters that are typically sorted to the vacuole upon ubiquitination, appears to have the opposite effect. Directing catalytic activity of deubiquitinating enzymes (DUb) to cargo, either directly or indirectly via Rsp5 or ESCRT proteins (Stringer and Piper, 2011; MacDonald et al., 2012a; b), antagonises cargo degradation and triggers recycling by default. To characterise this pathway, a genetic screen using a DUb fused version of the receptor Ste3 (Ste3-GFP-DUb) was performed to reveal 89 factors that are required for this recycling (MacDonald and Piper, 2017), most of which were validated with additional assays for Tat2 (Johnson et al., 2010) and FM4-64 (Wiederkehr et al., 2000) recycling. Null mutants of retrograde machinery like retromer, Snx4/41/42 and Ere1/2 (Seaman et al., 1998; Hettema et al., 2003; Shi et al., 2011) were not identified by the screen and recycle FM4-64 at similar rates to wild-type cells. Furthermore, cells harbouring a mutant allele of *SEC7* with abrogated trafficking through the Golgi also exhibit efficient DUb-triggered recycling. These data suggest the recycling of DUb-fused cargoes is predominantly distinct from retrograde recycling of Snc1, but there is likely overlap between pathways as some endosomal machinery that Snc1 relies on was shown to be required for Ste3-GFP-DUb recycling (e.g. Rcy1, Cdc50-Drs2, Ypt31/32).

This genetic screen also implicated Ist1 in the yeast endosomal recycling pathway triggered by cargo deubiquitination. Ist1 shares structural homology with other ESCRT-III subunits and contributes to the efficiency of MVB sorting (Dimaano et al., 2008; Rue et al., 2008; Xiao et al., 2009; Frankel et al., 2017; Buono et al., 2016; Pfitzner et al., 2020). Ist1 interacts with other ESCRT-III subunits and Vps4, the AAA-ATPase required for MVB sorting and disassembly of ESCRT polymers (Babst et al., 1997, 1998, 2002; Nickerson et al., 2006; Azmi et al., 2006). Ist1 regulation of Vps4 is complex, even *in vitro* Ist1 can stimulate and inhibit Vps4 activity and control depends on other ESCRT-III subunits (Tan et al., 2015). Therefore, despite great strides in our understanding of ILV formation by ESCRT-III filaments and Vps4 (Han et al., 2017; Adell et al., 2017; Maity et al., 2019; Pfitzner et al., 2020) our understanding of the role(s) of Ist1 in the endosomal assemblage of ESCRTs *in vivo* is incomplete. Furthermore, high levels of Ist1 inhibit MVB sorting and diverse cargoes are sorted more efficiently to the vacuole in *ist1*Δ cells (Dimaano et al., 2008; Jones et al., 2012). In addition to the negative regulation of Vps4, it may be that Ist1 also promotes an opposite acting recycling pathway to the PM. In support of this idea, *in vivo* and *in vitro* studies show that unlike ESCRT-III polymers, which drive luminal vesicle formation, Ist1 polymerisation, in combination with CHMP1B, exerts the opposite effect on endosomal membranes to generate tubulation of cytosolic protrusions (McCullough et al., 2015; Nguyen et al., 2020). Physiologically this can be best rationalised by Ist1 promoting the recycling pathway by creation / fission of recycling tubules that return material back to the PM. Cellular work has suggested this occurs in collaboration with the ATPase spastin (Allison et al., 2013, 2017), but reconstitution of the process *in vitro* shows ESCRT assemblies in combination with a mechanical pulling force is sufficient to drive scission (Cada et al., 2022).

In this study we present evidence that, as expected, the surface cargoes Snc1/2 mainly follow a trafficking route to the TGN labelled with the Arf-exchange factor Sec7. However, this trafficking appears to be distinct from the pathway used by nutrient transporters for methionine (Mup1) and uracil (Fur4). Upon addition of substrate, nutrient transporters rapidly internalize to compartments marked by Vps4 and Ist1, followed by delivery to the vacuole. However, using microfluidics to rapidly remove the substrate-induced ubiquitin-degradation signal, Mup1 recycles directly back to the PM from this Vps4 endosome population. These trafficking events are not observed to transit Sec7-labelled TGN compartments. This recycling pathway driven by cargo deubiquitination relies on the ESCRT-III associated protein Ist1. We provide initial evidence that Ist1 is ubiquitinated and this is required for its ability to recycle cargoes back to the PM. We also reveal Npl4-Cdc48 is required for proper endosomal regulation of Ist1 mediated cargo recycling.

RESULTS & DISCUSSION

Differential cargo recycling routes in yeast

The v-SNARE Snc1 is a well-established retrograde cargo that internalizes and recycles via the TGN back to the plasma membrane (PM) through multiple pathways (Lewis et al., 2000; Best et al., 2020). Snc1 ubiquitination is required for recycling (Xu et al., 2017) and the fusion of the catalytic domain of a deubiquitinating enzyme (DUb) is sufficient to block recycling of GFP-tagged Snc1 and the paralogue Snc2 (**Fig. 1A**). In contrast, substrate induced ubiquitination of the Mup1 (methionine) or Fur4 (uracil) permeases does not promote recycling and instead drives endocytosis and vacuolar degradation (Menant et al., 2006; Lin et al., 2008; Hein et al., 1995; Keener and Babst, 2013). Mup1-GFP localizes to the surface but is almost entirely sorted to the vacuole within 1-hour after methionine addition. This ubiquitin-dependent sorting is blocked by a DUb-fusion to Mup1-GFP (**Fig. 1B**). Similarly, although Fur4 steady state localization includes intravacuolar signal, any surface localized Fur4 is sorted to the vacuole in the presence of uracil, and this trafficking is blocked by DUb-fusion.

Retrograde recycling of Snc1/2 via the TGN is required for its polarised PM distribution (Lewis et al., 2000; Valdez-Taubas and Pelham, 2003; Hettema et al., 2003; Ma et al., 2017), with GFP tagged Snc1/2 concentrated in budding daughter cells (**Figs. 1C - 1E**). Unlike Snc1/2, fluorescently tagged Mup1 and Fur4 concentrate in the mother cell during budding (**Figs. S1A - S1E**). This polarisation is maintained throughout the cell cycle for cells expressing Fur4 but only obvious in small cells (<2.5 µm diameter) expressing Mup1, with the levels increasing to roughly the same as mother cells later in the cell cycle. As Snc1/2 is the R-SNARE carried on secretory vesicles that feed material into the growing daughter cell, it would be expected to transit the Golgi. However, nutrient transporters may not provide physiological benefit to burgeoning daughter cells, as their surface residence is maintained by recycling in only mother cells.

As expected, intracellular signal from retrograde cargoes Snc1/2 tagged with GFP colocalizes with the TGN marker Sec7-mCherry, with very little overlap with the endosomal marker Vps4-mCherry (**Fig. 1F**). Furthermore, DUb-GFP-Snc1/2 fusions, which do not recycle efficiently, accumulate in Sec7-marked TGN compartments (**Fig. 1G**). The majority of intracellular signal is contributed by recycling Snc1, and not first-pass molecules transiting the Golgi, as a mutant version of Snc1 ($Snc1^{PM}$) with defective internalization (Lewis et al., 2000) exhibits very little intracellular signal, which maintains colocalization with Sec7-mCherry (**Fig. 1H**). In contrast, intracellular Mup1-GFP, triggered by a 5-minute exposure to methionine or by nutrient starvation experienced in cells grown to late log-phase (MacDonald et al., 2012b, 2015), primarily internalises to Vps4-mCherry, and not Sec7-positive TGN, compartments (**Fig. 1I**). Similarly, Fur4-mNG that has significant intracellular signal irrespective of substrate presence colocalizes with Vps4 endosomes (**Fig. 1J**). Although cargo-specific trafficking regulation might explain mother-daughter differences, taken with the opposing effects of enforced deubiquitination and differences in intracellular localization, we propose that endosomal recycling of nutrient transporters follows a distinct route than that used by Snc1/2 via the Golgi (**Fig. 1K**).

Nutrient transporters recycle from early endosomes

Although enforced deubiquitination of internalized nutrient transporters promotes their recycling to the surface, observing recycling of unmodified nutrient transporters is hampered by their proclivity for vacuolar sorting (Stringer and Piper, 2011; MacDonald et al., 2012a; b, 2015). To overcome this, we optimised microfluidic exchange with continuous imaging to perform a substrate pulse, followed by washes and substrate-free chase to allow internalized cargo to recycle naturally (**Fig. 2A**). Mup1-GFP was used for these experiments as it exhibits steady state localization at the PM, and we found high (40 µg/ml) and low (2 µg/ml) levels of methionine triggered accumulation of intracellular puncta, with high doses giving brighter, more obvious puncta (**Fig. 2B**). The pulse-chase protocol resulted in accumulation of intracellular Mup1-GFP for 0-15 minutes followed by clearance of most signal after an additional 15 minutes, regardless of methionine pulse concentration. To avoid concerns about photobleaching or substrate induced degradation, biochemical analysis was used to show that methionine pulse periods of 1 or 5 minutes, followed by substrate free chase up to 60 minutes resulted in no increase in vacuolar delivery of internalized material (**Figs. 2C - 2D**). All subsequent substrate induced experiments were performed with <1 minute methionine pulses. To confirm intracellular nutrient transporter signal emanated from the surface, we optimised photoconversion of surface localized Mup1-mEos and Fur4-mEos (**Figs. 2E - 2F**). Coupling cargo photoconversion to microfluidic induced recycling and time-lapse microscopy, revealed signal of intracellular Mup1 that has trafficked from the PM, which subsequently dissipates with similar kinetics to Mup1-GFP (**Fig. 2G, Movie S1**). We then followed the trafficking itinerary of internalized and recycled Mup1-GFP using 4D confocal Airyscan microscopy optimised for rapid acquisitions. Methionine induced internalization tracked at 4 - 10 second intervals show substantial intracellular accumulations that colocalize with Vps4-mCherry, and not Sec7-mCherry, within the first few minutes (**Fig. 3A, Movies S2 - S3**). Additionally, Mup1-GFP recycling experiments were imaged over longer periods to show Mup1 primarily traverses Vps4 endosomes, bypassing Sec7-mCherry compartments (**Figs. 3B - 3C, Movie**

S4-S5). We also tracked colocalization from time-lapse imaging experiments and find Mup1-GFP almost exclusively colocalizes with Vps4-mCherry over time (Fig. 3D-3E). We further note that the small levels of colocalization detected between Mup1-GFP and Sec7-mCherry were only observed when Sec7 signal was adjacent to the PM (Fig. 3F). This marginal level of colocalization with peripheral Golgi compartments may have derived from PM localized Mup1-GFP following deconvolution, and not an internalized endosome population.

Ist1 is required for cargo recycling

Vps4, the ATPase involved in ESCRT-mediated ILV formation, marks a large and relatively static endosome reminiscent of Vps8 compartments (Day et al., 2018) in addition to a population of peripheral mobile compartments (Adell et al., 2017). The ESCRT-associated factor Ist1 colocalizes with Vps4 in both populations, in addition to potentially distinct endosomes (Figs. 4A - 4B, Movie S6). It is tempting to speculate that the large static endosome population of Vps4, which is also termed the prevacuolar compartment due to its vicinity to the vacuole, represents functionally definable MVBs. Other Vps4 and Ist1 positive compartments might be more akin to sorting or recycling endosomes, which have not matured or committed to ILV formation and surface protein degradation. As Ist1 was the only recycling factor from a blind genetic screen of ~5200 mutants (MacDonald and Piper, 2017) that also interacts with Vps4 (Fig. 4C), and its orthologues have been implicated in recycling (Allison et al., 2013; Frankel et al., 2017; McCullough et al., 2015), we hypothesised Ist1 might functionally define this population of recycling endosomes. We integrated the Ste3-GFP-DUb recycling reporter to confirm recycling defects of *ist1*Δ and *rcy1*Δ cells, in addition to quantifying their capacity for recycling Tat2 and FM4-64 (Figs. 4D - 4F). Deletion of *ist1*Δ in cells expressing Mup1-GFP caused recycling defects, with a small population of Mup1-GFP retained in endosomes marked by Vps4-mCherry and distinct from Sec7-mCherry positive compartments (Fig. 4G).

Npl4-Cdc48 regulates Ist1-recycling

As the mammalian orthologue of yeast Ist1 has been implicated in polymerisation and creation of cytosolic recycling tubules (McCullough et al., 2015; Allison et al., 2013, 2017), we reasoned this function could be conserved in yeast (Fig. 5A). Vps4 is an obvious candidate AAA-ATPase for Ist1 depolymerisation. However, *vps4*Δ cells exhibit only a marginal defect in FM4-64 recycling (MacDonald and Piper, 2017) and a mutant of Ist1 ($Ist1^{\Delta MIM}$) with significantly diminished Vps4-binding (Dimaano et al., 2008; Tan et al., 2015) rescues efficient FM4-64 recycling of *ist1*Δ cells (Fig. 5B). Encouragingly, a similar mutation to mammalian Ist1 lacking Vps4-binding has recently been shown to function in membrane deformations that would be required for recycling (Cada et al., 2022). Other Ist1 mutants ($Ist1^{K52D}$, $Ist1^{K74A}$, and $Ist1^{K135A}$) that are defective in regulating Vps4 (Tan et al., 2015) also recycle FM4-64 with no obvious defects when compared with wild-type Ist1 (Fig. S2A). This suggests that Vps4 has no major or direct role in cargo recycling. This idea is supported by the observation that *vps4* mutants, both *vps4*Δ nulls or cells expressing dominant negative $Vps4^{EQ}$ allele, that are defective in sorting the MVB cargo Cos5-GFP have no impact on recycling Ste3-GFP-DUb efficiently (Fig. 5C). Collectively, this implies that the Vps4 ATPase required for ILV formation during cargo degradation can be functionally separated from Ist1-mediated cargo recycling from endosomes back to the PM.

Screening for recycling machinery did not identify any other ATPase candidates but did implicate Npl4, an adaptor of the essential Cdc48 ATPase, as required for recycling (Figure S2B). We demonstrate that both Npl4 (Figs. 5D - 5E) and Cdc48 (Figs. 5F - 5G) are required to efficiently recycle Ste3-GFP-DUb and FM4-64 back to the PM. This led to our speculative model that the role of Cdc48-Npl4 in recycling was mediated via Ist1. In support of this idea, deletion of *IST1* in either a *npl4*Δ or *cdc48-2* mutant backgrounds did not result in further deficiency in recycling FM4-64 (Figs. 5H - 5I), which would be predicted if Ist1 did function in the same pathway.

Ist1 is ubiquitinated

We extended this hypothetical model that functionally connects Ist1 to Npl4-Cdc48 (Fig. 6A), predicting that Ist1 ubiquitination would allow Cdc48 recruitment via the well-established Npl4-ubiquitin binding motif (Wang et al., 2003). Although Ist1 is known to be turned over by the proteasome (Jones et al., 2012), it has not been formally demonstrated to be ubiquitinated, likely owning to the abundance of Lys / Arg residues in its sequence, that represent 50/298 amino acids (Fig. 6B). Commonly used enzymes upstream of mass-spectrometry, like Trypsin and LysC, cleave at Lys/Arg residues and would promote extensive digestion and reduce likelihood of identifying ubiquitin modified peptides by mass-spectrometry (Swaney et al., 2010). In an effort to identify *bona fide* Ist1 ubiquitination sites we created an endogenously tagged version of Ist1 with a C-terminal HA tag and a His_6 tag to allow purification under denatured conditions (Fig. 6C). Purification from 2 litres of cultures grown to log phase provide high levels of Ist1 enrichment by immunoblot, including protein species evident by Coomassie staining at this approximate molecular weight (Fig. 6D). However, in gel digestion of these bands followed by analysis using Matrix Assisted Laser Desorption/Ionization (MALDI) mass spectrometry revealed these were not Ist1 (Fig. S3A).

Instead, the purified eluates were prepared for Liquid Chromatography with tandem mass spectrometry (LC-MS/MS) using an optimised protocol aimed at identifying ubiquitinated Ist1 peptides (**Fig. 6E**). This included the sequential digest by ArgC followed by acidification and digest with ProAlanase. Half the sample was also subjected to propionylation, which has previously been shown to increase the hydrophobicity and retention of lysine containing peptides prior to mass spectrometry (Drury et al., 2012). This revealed many previous yeast contaminants from denatured lysates (**Fig. S3B**), thousands of unique peptides (**Supplemental Table T5**), in addition to several distinct Ist1 peptides (**Fig. 6F**). One spectrum matched as a ubiquitin remnant modified peptide (diGly), even at 5% false discovery rate (FDR). However, due to low intensity the spectra could not be manually confirmed. Furthermore, the fact that Ist1 has 38 lysines residues spread across only 298 amino acids, almost double than the average across the yeast proteome (**Figs. S3C**), multiple redundant ubiquitination sites are possibly retained.

As an alternative approach we performed a denatured ubiquitome purification using an optimised strain expressing His_6 tagged ubiquitin (MacDonald et al., 2017) to reveal that ubiquitinated species of Ist1 can be observed (**Figs. 6G, S3D**). We believe this pull-down result represents ubiquitinated Ist1, as a repeat in *ist1*Δ mutant strain shows similar levels of purified material and non-specific bands, but no Ist1 at its predicted molecular weight (**Fig. 6H**). Collectively, this data suggest that Ist1 is ubiquitinated and we provide initial evidence that minimally K135, which is highly conserved across evolution (**Fig. S3E**), might serve as a ubiquitination site.

Ubiquitinated Ist1 is required for recycling

Our model would predict that ubiquitination of Ist1 is required for recycling, promoting recruitment of Cdc48 via Npl4 (**Fig. 6A**). To explore this hypothesis in more detail, we created HA tagged versions of wild-type ($Ist1^{WT}$-HA) and a mutant resistant to ubiquitination ($Ist1^{KR}$-HA), which has all 38 lysine residues mutated to arginine. Although levels of $Ist1^{KR}$-HA are somewhat reduced (**Fig. 7A**), a cycloheximide chase to inhibit translation reveals that it has similar stability to $Ist1^{WT}$-HA over a 2-hour chase period (**Figs. 7B - 7C, S4A - S4C**). Similarly, not only does the mutant $Ist1^{KR}$ tagged with GFP persist in cells, but it localizes to Vps4-positive endosomes that are distinct from Sec7 compartments (**Figs. 7D - 7E**). Although $Ist1^{KR}$ mutants have similar behaviour, only $Ist1^{WT}$-HA supports the recycling defect Mup1-GFP expressed in *ist1*Δ cells, with Mup1-GFP retained at Vps4-endosomes in cells expressing $Ist1^{KR}$-HA (**Fig. 7F**). Furthermore, only $Ist1^{WT}$-HA supports recycling of FM4-64 in *ist1*Δ cells to wild-type levels, but $Ist1^{KR}$-HA cannot (**Fig. 7G**).

Although our evidence implicates Ist1 ubiquitination in recycling, this approach to create a lysineless version necessitated a large number (38/298) of point mutations. To confirm the stability of $Ist1^{KR}$ *in vitro*, we optimised expression of His_6 tagged versions of $Ist1^{WT}$ and $Ist1^{KR}$ in bacterial cells (**Fig. S4D**). Recombinant $Ist1^{WT}$ and $Ist1^{KR}$ had similar yields and levels of purity (**Figs. 7H - 7I**). Analysing purified protein by nanoscale differential scanning fluorimetry (nanoDSF) detected aberrations in protein stability at similar stages of the heat ramp, with $Ist1^{WT}$ at 35.3 ± 3.2ºC and and $Ist1^{KR}$ at 38.5 ± 1.4ºC (**Figs. 7J - 7K**). Furthermore, analysis of the scattering profiles, an indirect measurement of aggregation during heat-induced unfolding, showed no obvious indication that either $Ist1^{WT}$ or $Ist1^{KR}$ were unstable at physiological temperature (**Figs. 7L - 7M**).

One caveat to the recycling defects observed above (**Fig. 7**) is that the $Ist1^{KR}$-HA mutant levels are lower than wild-type, so it is unclear whether reduced cellular protein levels or lack of ubiquitination sites in $Ist1^{KR}$ are responsible for defects in recycling. To distinguish between these possibilities, we took advantage of a Yeast Estradiol with Titratable Induction (YETI) system (Arita et al., 2021) that allows *IST1* expression to be controlled with titration of ß- estradiol / E2 (**Fig. 8A**). Optimising 6-hour E2 treatments and assessing Ist1 levels by immunoblot revealed conditions that mimic: *ist1*Δ cells with no E2 in the media; $Ist1^{WT}$ with 0.7 ± 0.4 nM, and $Ist1^{KR}$ = 0.2 ± 0.04 nM (**Fig. 8B - 8C**). We find that mimic of either $Ist1^{WT}$ or $Ist1^{KR}$ levels was sufficient to restore recycling of both Mup1-GFP and FM4-64 (**Fig. 8D - 8E**).

In support of a model for Ubiquitin > Npl4 > Cdc48 regulating endosomal cycling of Ist1, we find elevated endosomal retention of $Ist1^{KR}$-GFP, which cannot be ubiquitinated (**Figs. S5A - S5B**). Furthermore, elevated endosomal levels of Ist1-GFP are observed in *npl4*Δ cells and mutants with reduced Cdc48 ATPase activity. Combining the lysineless version of $Ist1^{KR}$-GFP with Npl4 / Cdc48 mutants results in its mislocalization to the nucleus (**Figs. S4C - S4D**), which precluded assessment of endosomal recruitment but further alludes to a biological connection between ubiquitinated Ist1 and Npl4-Cdc48. To better implicate Ist1 ubiquitination in recycling, we generated a DUb-fusion of Ist1-GFP and a catalytically inactive $dub^{C>S}$ counterpart (**Fig. 9A**). As expected, neither Ist1-GFP-DUb or Ist1-GFP- $dub^{C>S}$ localize with Sec7 compartments (**Fig. 9B, 9E**). In agreement with $Ist1^{KR}$ experiments, we find that Ist1-GFP-DUb is defective in recycling to the same degree as *ist1*Δ cells (**Fig. 9F**). Introducing only a single point mutation to ablate catalytic activity on the enzyme (Ist1-GFP- $dub^{C>S}$) is sufficient for the fusion protein to recycle FM4-64 to wild-type levels (**Fig. 9G**). Although perturbing Ist1-GFP ubiquitination by fusion with a DUb results in colocalization with the large, static prevacuolar Vps4 population, there is an observable separation of Vps4 and Ist1 in the small mobile population (**Fig. 9C -**

9E). This suggests that although Vps4 and Ist1 occupy the same compartments in wild-type conditions, that distinct trafficking intermediates can emanate from these endosomes to recycle material back to the surface.

Whilst it was expected that Sec7 would not localize to these recycling endosomes, it is curious that Ist1 compartments labelled by the non-functional Ist1-GFP-DUb, but lacking Vps4, are more obvious and numerous. The residence of Vps4 and Ist1 on overlapping endosome populations might allow fine tuning of the surface proteome, for example in response to metabolic demand. If cargo is destined for recycling from endosomes the role of Ist1 is prioritised but if sufficient ubiquitinated cargoes accumulate Vps4- and ESCRT coalescence (Banjade et al., 2022) predominates to drive cargo degradation.

SUMMARY

We show that retrograde recycling of Snc1/Snc2 is distinct from the recycling of the Mup1/Fur4 nutrient transporters. Snc1/2 mainly internalize to Sec7-marked TGN compartments, exhibit polarised distribution in daughter cells and rely on cargo ubiquitination (**Figure 1**). In contrast, Mup1/Fur4 internalize to Vps4-marked endosome compartments, localize predominantly to mother cells during budding, and deubiquitination triggers their recycling. Ubiquitination of nutrient transporters like Mup1 in response to substrate (Schothorst et al., 2013) can be counteracted by substrate removal, which triggers cargo recycling from Vps4 compartments back to the PM (**Figures 2 & 3**). Given Mup1 internalizes to Vps4 endosomes on the scale of seconds to minutes, these compartments can be considered yeast early endosomes. Furthermore, our interpretation of the imaging and biochemical data presented is internalized Mup1 recycles back to the surface directly from these endosome compartments, allowing them to be considered as yeast recycling endosomes. Although endosomal recycling of cargo in mammalian cells is complex (Grant and Donaldson, 2009; Goldenring, 2015; O'Sullivan and Lindsay, 2020), these observations support the notion that recycling features are evolutionarily conserved and can be elucidated using yeast.

To this end, we reveal mechanisms of action of the yeast orthologue of mammalian IST1, which regulates endosomal recycling in animal cells (McCullough et al., 2015; Allison et al., 2013, 2017). We demonstrate that yeast Ist1 is required for recycling of proteins and lipids back to the PM (**Figure 4**). We find Ist1 is ubiquitinated (**Figure 6**) and a lysineless $Ist1^{KR}$ is not functional in endosomal recycling, due to its lack of ubiquitin sites (**Figure 7 - 8**). Beyond this, we used a ubiquitination reversal strategy that also demonstrated that Ist1 ubiquitination is required for recycling (**Figure 9**). Recently, regulation of the IST1 partner CHMP1B has also been shown through ubiquitination (Crespo-Yàñez et al., 2018), alluding to a general posttranslational means to control ESCRT-polymerisation in other modes of actions. Super resolution imaging, especially combined with the DUb fusion strategy to inhibit Ist1-mediated recycling, shows that non-Golgi Ist1-endosomes can be observed +/- Vps4, further alluding to complexity of endosomal organisation in yeast.

In addition to ubiquitination of Ist1, we show the ubiquitin-binding adaptor Npl4 and its ATPase partner Cdc48 (p97 / VCP) regulate endosomal recruitment of Ist1 and are required for efficient cargo recycling to the PM (**Figure 5**). It may be that the role of Ist1 in yeast recycling depends on its polymerisation, analogous to its mammalian counterpart. The most likely functional connection to Ist1 ubiquitination being required for recycling is via the ubiquitin-binding protein Npl4 and Cdc48, especially as combining these mutations does not exacerbate recycling defects (**Figure 5**). This speculative model collectively unites many trafficking observations in different systems and argues conserved mechanisms drive distinct yeast recycling pathways.

METHODS

Reagents

Supplemental tables are included to document use of plasmids (**Supplemental Table T1**), yeast strains (**Supplemental Table T2**), and primary antibodies (**Supplemental Table T3**).

Cell culture

Saccharomyces cerevisiae yeast strains were cultured in synthetic complete minimal media (SC; 2% glucose, yeast nitrogen base supplemented with base / amino acid drop out mixtures for selections) or yeast extract peptone dextrose (YPD; 2% glucose, 2% peptone, 1% yeast extract). Yeast cultures were typically grown in serial dilution overnight to allow for harvesting at mid-log phase ($OD_{600} \leq 1.0$) prior to experimentation, unless otherwise stated. Selection for strains harbouring KanMX cassettes were carried out in rich media containing 250 µg/ml geneticin/G418 (Formedium). The mCherry and GFP fusions of *SEC7* were generated with a methotrexate cassette selected on SC media containing 20 mM methotrexate (Alfa Aesar) and 5 mg/ml sulphanilamide before the *loxP* flanked cassette was excised by transient expression from a *TEF1-Cre* plasmid that was subsequently removed via 5-Fluoroorotic Acid media (MacDonald and Piper, 2015) Expression from

the *CUP1* promoter was induced by the addition of 20 - 100 μM copper chloride. Methionine (20μg/ml) and uracil (40 μg/ml) were added to SC media to induce trafficking of Mup1 and Fur4, respectively. Cycloheximide chase experiments were performed using yeast harbouring a *pdr5Δ* mutation grown to mid-log phase in SC media followed by growth in media containing 25mg/L cycloheximide form indicated time points prior to lysate generation. Yeast Estradiol Titratable Induction (YETI) control of *IST1* was achieved by addition of indicated concentrations of β-estradiol to SC growth media from for 6 hours.

Confocal microscopy

Yeast cells were harvested from early-mid log phase ($OD_{600} \leq 1.0$) and prepared for imaging using Zeiss laser scanning confocal instruments (typically LSM880 equipped with an Airyscan or LSM780/LSM710) using the Plan-Apochromat 63x/1.4 objective lenses. The fluorescent proteins mCherry, photo-converted mEOS and mStrawberry were excited using the 561 nm line from a yellow DPSS laser and the emission range 570-620 nm was collected. The fluorescent proteins mGFP, GFP, mNeonGreen and pre-converted mEOS were excited using the 488nm line from an Argon laser, the emission range 495-550 nm was collected. The fluorescent protein mEOS was photo converted using 0.5% the 405nm laser with 5 iterations per conversion and 3 conversions of a defined region of interested as stated. YPD containing 0.8 μM FM4-64 was used to label vacuoles for 1-hour followed by 3x washing and 1-hour chase period in SC minimal media. For dual population imaging, cultures were grown independently to mid log phase before mixing 1:1 ratio and grown for a further 1-3 hours. 5 μg/ml Hoescht was added to harvested cells for 10 minutes prior to imaging, and was excited using the 405nm line, the emission 460/50 nm was collected.

Microfluidics and time-lapse microscopy

Yeast cultures were grown to very early log phase ($OD_{600} \leq 0.2$) and adhered to 35 mm glass bottom coverslip dishes (Ibidi GmbH, Germany) coated with concavalin A (Sigma-Aldrich) prior to live-cell imaging at room temperature. Concavalin A coating was prepared by adding 1 mg/ml concavalin A in water to the glass bottom coverslip for 5 minutes prior to three washing steps; prepared plates were routinely stored at 4°C. Sterile media exchanges were performed using 50mL syringes through tubing fused to the lid of the 35 mm dishes.

Image analysis

Airyscan micrographs were processed using Zen software (Zeiss) and were further modified using Fiji. For time-lapse movies, bleach correction was carried out using the inbuilt Fiji plugin and histogram-matching method (Miura, 2020). Any necessary drift correction was carried out in Fiji using the plugins Hyper Stack Reg and Turbo Reg (Thevenaz et al., 1998). Fluorescence intensity measurements during photoconversion experiments was assessed in Zen Black. Steady state colocalization measurements of cells expressing Mup1-GFP in **Figure 3C** were performed using cell magic wand and morphological erosion to exclude surface signal prior to Pearson correlation coefficients being calculated. For other colocalization analyses, as indicated Mander's overlap coefficients or Pearson's correlation coefficients were calculated using Zen Blue / Zen Black (Zeiss) following normalisation for cells expressing individual GFP and mCherry fluorescent proteins. Immunoblot intensities were measured using imageJ and normalised to background and GAPDH signal. To estimate percentage endosome GFP signal, the intensity was compared from endosomes segmented using otsu thresholding and from the whole cell. All data was then plotted in GraphPad (v9.0.2, Prism).

FM4-64 recycling assay

Yeast cultures were grown to mid-log phase in SC minimal media with corresponding selection to plasmid or YPD, 1 mL of cells (OD = 1.0) were harvested, incubated for 8 min at room temperature in 100 μL YPD containing 40 μM FM4-64 dye (*N*-(3-Triethylammoniumpropyl)-4-(6-(4-(Diethylamino) Phenyl) Hexatrienyl) Pyridinium Dibromide) dye. Labelled cells were then washed in ice cold SC media for 3 minutes on ice, 3 times. Final wash concentrated cells in 100 μL SC media in preparation for flow cytometry. Approximately 2500 cells were flowed per second at ~600 V using LSR Fortessa (BD Biosciences), over a 10 min time period the FM4-64 intensity was measured with excitation 561 nm, laser filter 710 / 50. Background autofluorescence was recorded using measurements from the 530 / 50 nm detector.

Immunoblotting

Equivalent amounts of yeast culture grown to mid log phase (OD_{600} = < 1.0) were harvested, treated with 500 μl 0.2 N NaOH for 3 minutes then resuspended in lysis buffer (8 M Urea, 10% glycerol, 5% SDS, 10% 2-Mercaptoethanol, 50mM Tris.HCl pH 6.8, 0.1% bromophenol blue). Proteins were resolved using SDS-PAGE and transferred to nitrocellulose membrane using the iBlot2 transfer system (ThermoFisher). The membrane was probed using the labelled antibodies and visualised using super signal Pico Plus (ThermoFisher) Enhanced chemiluminescence signal intensity was captured using an iBright^{TM} Imager (ThermoFisher).

Statistical tests
Indicated statistical tests for experimental comparisons were performed using GraphPad (v9.0.2, Prism). An asterisk is used in graphs to denote statistically significant differences. Statistical tests used throughout the manuscript and p values are shown in **Supplemental Table T4**).

Bioinformatics
Gene ontology term finder(Cherry et al., 2012) was used to analyse all the results of the genetic screen for recycling machinery described in(MacDonald and Piper, 2017) with searches for specific enzyme activity shown. The physical interactome was acquired from YeastMine (Balakrishnan et al., 2012)

Tat2 recycling assay
Tryptophan auxotroph (*trp1Δ)* yeast cells were grown to mid log-phase before being spotted out across a 10-fold serial dilution and grown on plates of indicated Tryptophan concentrations. Yeast growth was normalised from a wild-type control on the same plate and used the calculate the growth difference, as previously described (Paine et al., 2021).

Protein purification from yeast
Yeast CMY158 and CMY2056 optimised for ubiquitin purification (MacDonald et al., 2017, 2020) expressing His_6-tagged ubiquitin, or yeast CMY2042 expressing Ist1-HA-His_6 were grown in a 2 L culture to mid-log phase before it was harvested and treated with 0.2 M NaOH for 3 minutes and brought up in denaturing lysis buffer (8 M urea, 20mM Sodium Phosphate pH 7.4, 300mM NaCl, 2.5% SDS, 5mM 2-mercaptoethanol). The lysates were diluted 80-fold using dilution buffer (8 M urea, 20mM Sodium Phosphate pH 7.4, 300mM NaC, 5mM 2-mercaptoethanol) and bound to 2 ml bed of Ni^{2+}-NTA agarose beads for 2 hours at room temperature. Beads were incubated with wash buffer (8 M urea, 20mM Sodium Phosphate pH 7.4, 300mM NaC, 5mM 2-mercaptoethanol, 5mM imidazole) 5 times before eluting using wash buffer at pH 4.5. The sample was then neutralised, bound to 100 µl bed of Ni^{2+}-NTA agarose beads for 2 hours, before repeat washes and elution in dilution buffer containing 500 mM imidazole. Loading buffer was added to the samples for downstream SDS-PAGE analysis.

Recombinant protein expression and purification
Protein expression for His_6-Ist1^{WT} and His_6-Ist1^{KR} was performed using BL21-DE3 (Invitrogen) and BL21-CodonPlus (Agilent) *Escherichia coli* strains grown in 1 L of LB broth to OD_{600} = 0.6 before induction with 0.5mM Isopropyl ß-D-1-thiogalactopyranoside (IPTG) for 16 hrs at 15°C. The cell pellet was resuspended in buffer A (20mM Sodium Phosphate pH 7.4, 300mM NaCl, 30mM Imidazole) containing cOmplete™ protease inhibitor cocktail (Roche) and sonicated, the lysate was clarified 18,000 x *g* and bound to 600 µl bed of Ni^{2+}-NTA agarose beads for 2 hrs at 4°C. Beads were washed 5x using 10mL buffer A before elution with buffer B (20mM Sodium Phosphate pH 7.4, 300mM NaCl, 500mM Imidazole). Protein concentrations assays were performed using Pierce™ BCA Protein Assay Kit (Thermo Scientific™), incubated at 37°C for 30 minutes before OD was measured at 560nm.

Differential Scanning Fluorimetry
Prometheus NT.48 instrument (NanoTemper Technologies) performed differential scanning fluorimetry (DSF) to determine T_m and T_{onset} of loaded protein samples. Purified protein samples in 20mM Sodium Phosphate pH 7.4, 300mM NaCl, 500mM Imidazole was loaded in nanoDSF grade standard capillaries (NanoTemper Technologies) and laser power optimised for signal. Thermal stress from 20°C to 95°C was performed on the sample shifting at a rate of 1°C per minute. Fluorescence emission from the single Ist1 tryptophan (W134) after excitation with UV at 280nm was collected at 330-350nm. Aggregation of protein was assessed concurrently with back reflection optics. Thermal stability parameters T_m and T_{onset} were unbiasedly assessed and calculated by PR. ThermControl software (V.2.1.3).

Matrix Assisted Laser Desorption/Ionization (MALDI) mass spectrometry
Proteins were digested from gels with 0.02 µg/µL modified porcine trypsin (Promega) after reduction with dithioerythritol and iodoacetamide, washing two times with 50% (v:v) aqueous acetonitrile containing 25 mM ammonium bicarbonate, then once with acetonitrile and dried in a vacuum concentrator for 20 min. Trypsin digests were incubated at 37°C before 1µL of peptide mixture was applied directly to the ground steel MALDI target plate, followed immediately by an equal volume of a freshly-prepared 5 mg/mL solution of 4-hydroxy-α-cyano-cinnamic acid (Sigma) in 50% aqueous (v:v) acetonitrile containing 0.1% , trifluoroacetic acid (v:v). Positive-ion MALDI mass spectra were acquired over a mass range of m/z 800-5000 using a Bruker ultraflex III in reflectron mode, equipped with a Nd:YAG smart beam laser. Spectral processing and peak list generation for MS and MS/MS spectra was performed with Bruker flexAnalysis software (version 3.3). Tandem mass

spectral data were searched with Mascot (Matrix Science Ltd., version 2.6.1), through the Bruker BioTools interface (version 3.2), against the *Saccharomyces cerevisiae* subset of SwissProt. Peptide spectral matches were filtered to require an expect score of 0.05 or better.

Liquid Chromatography with tandem (LC-MS/MS) mass spectrometry

Denatured protein was diluted to 2 M urea with aqueous 50 mM ammonium bicarbonate, reduced with 0.7 mg/mL dithiothreitol and heating at 55ºC, then alkylated with 1.9 mg/mL chloroacetic acid before proteolytic digestion with 0.2 µg sequencing grade ArgC (Promega) and incubation at 37ºC for 16 h. Peptide solution was then acidified to 0.1% formic acid before adding 0.2 µg Mass Spec grade ProAlanase protease (Promega) and incubating at 37ºC for a further 2 h. Resulting peptides were desalted using C_{18} ZipTip filters (Millipore), eluted with 50% acetonitrile, dried under vacuum. Half the peptide mixture was adjusted to pH 10 with ammonium hydroxide, 10 µL of propionic anhydride was added and sample incubated at 60 ºC for 1 h. The other peptide mixture was not propionylated. Both sets of peptides were acidified with 0.1% trifluoroacitic acid, vacuum dried and re-dissolving in aqueous 0.1 % (v:v) trifluoroacetic acid followed by analysis by LC-MS/MS. Peptides were loaded onto an mClass nanoflow UPLC system (Waters) equipped with a nanoEaze M/Z Symmetry 100 Å C_{18}, 5 µm trap column (180 µm x 20 mm, Waters) and a PepMap, 2 µm, 100 Å, C_{18} EasyNano nanocapillary column (75 µm x 500 mm, Thermo).

Separation used gradient elution of two solvents: solvent A, aqueous 0.1% (v:v) formic acid; solvent B, acetonitrile containing 0.1% (v:v) formic acid. The linear multi-step gradient profile was: 3-10% B over 7 mins, 10-35% B over 30 mins, 35-99% B over 5 mins and then proceeded to wash with 99% solvent B for 4 min. The nanoLC system was interfaced with an Orbitrap Fusion Tribrid mass spectrometer (Thermo) with an EasyNano ionisation source (Thermo). Positive ESI-MS and MS^2 spectra were acquired using Xcalibur software (version 4.0, Thermo). Instrument source settings were: ion spray voltage, 1,900 V; sweep gas, 0 Arb; ion transfer tube temperature; 275°C. MS^1 spectra were acquired in the Orbitrap with: 120,000 resolution, scan range: *m/z* 375-1,500; AGC target, $4e^5$; max fill time, 100 ms. Data dependent acquisition was performed in top speed mode using a 1 s cycle, selecting the most intense precursors with charge states >1. Dynamic exclusion was performed for 50 s post precursor selection and a minimum threshold for fragmentation was set at $5e^3$. MS^2 spectra were acquired in the linear ion trap with: scan rate, turbo; quadrupole isolation, 1.6 *m/z*; activation type, HCD; activation energy: 32%; AGC target, $5e^3$; first mass, 110 *m/z*; max fill time, 100 ms. Acquisitions were arranged by Xcalibur to inject ions for all available parallelizable time.

Peak lists were analysed using PEAKS StudioX Pro (Bionformatic Solutions Inc.) and Byonic (Protein Metrics) against the *Saccharomyces cerevisiae* subset of SwissProt. Peptide identifications were adjusted to achieve a 5% false discovery rate as assessed empirically against a reverse database search.

ACKNOWLEDGMENTS

We would like to thank Dave Katzmann (Mayo Clinic) for Ist1 antibodies and expression plasmids; David Teis (University of Innsbruck) and Jeff Brodsky (University of Pittsburgh) for yeast strains; Rob Piper (University of Iowa), Markus Babst (University of Utah), and Chris Stefan (LMCB, UCL) for helpful discussions. Thanks also to staff at York Bioscience Technology Facility, in particular Pete O'Toole, Jo Marrison, Karen Hogg and Graeme Park for help with imaging and photoconversion. Thanks to Jared Cartwright (Protein Production Laboratory) for advice on protein purification and Andrew Leech (Molecular Interactions Laboratory) for nanoDSF training. Thanks also to Adam Dowle and Chris Powell (Centre of Excellence in Mass Spectrometry) for help with proteomics. Finally, thanks to Sarah Lecinski for advice on data analysis and Katherine Paine for comments on the manuscript. This research was supported by a Sir Henry Dale Research Fellowship from the Wellcome Trust and the Royal Society 204636/Z/16/Z (CM).

DECLARATION OF INTERESTS

The authors declare no competing interests.

REFERENCES

Adell, M.A.Y., S.M. Migliano, S. Upadhyayula, Y.S. Bykov, S. Sprenger, M. Pakdel, G.F. Vogel, G. Jih, W. Skillern, R. Behrouzi, M. Babst, O. Schmidt, M.W. Hess, J.A. Briggs, T. Kirchhausen, and D. Teis. 2017. Recruitment dynamics of ESCRT-III and Vps4 to endosomes and implications for reverse membrane budding. *Elife*. 6:e31652. doi:10.7554/elife.31652.

Allison, R., J.R. Edgar, G. Pearson, T. Rizo, T. Newton, S. Günther, F. Berner, J. Hague, J.W. Connell, J. Winkler, J. Lippincott-Schwartz, C. Beetz, B. Winner, and E. Reid. 2017. Defects in ER-endosome contacts impact lysosome function in hereditary spastic paraplegia. *J Cell Biol*. 216:1337 1355. doi:10.1083/jcb.201609033.

Allison, R., J.H. Lumb, C. Fassier, J.W. Connell, D.T. Martin, M.N.J. Seaman, J. Hazan, and E. Reid. 2013. An ESCRT-spastin interaction promotes fission of recycling tubules from the endosome. *J Cell Biology*. 202:527 543. doi:10.1083/jcb.201211045.

Arita, Y., G. Kim, Z. Li, H. Friesen, G. Turco, R.Y. Wang, D. Climie, M. Usaj, M. Hotz, E.H. Stoops, A. Baryshnikova, C. Boone, D. Botstein, B.J. Andrews, and R.S. McIsaac. 2021. A genome-scale yeast library with inducible expression of individual genes. *Mol Syst Biol*. 17:e10207. doi:10.15252/msb.202110207.

Azmi, I., B. Davies, C. Dimaano, J. Payne, D. Eckert, M. Babst, and D.J. Katzmann. 2006. Recycling of ESCRTs by the AAA-ATPase Vps4 is regulated by a conserved VSL region in Vta1. *J Cell Biology*. 172:705 717. doi:10.1083/jcb.200508166.

Babst, M., D.J. Katzmann, E.J. Estepa-Sabal, T. Meerloo, and S.D. Emr. 2002. Escrt-III: an endosome-associated heterooligomeric protein complex required for mvb sorting. *Developmental Cell*. 3:271 282. doi:10.3410/f.1009409.126008.

Babst, M., T.K. Sato, L.M. Banta, and S.D. Emr. 1997. Endosomal transport function in yeast requires a novel AAA-type ATPase, Vps4p. *Embo J*. 16:1820 1831. doi:10.1093/emboj/16.8.1820.

Babst, M., B. Wendland, E.J. Estepa, and S.D. Emr. 1998. The Vps4p AAA ATPase regulates membrane association of a Vps protein complex required for normal endosome function. *Embo J*. 17:2982 2993. doi:10.1093/emboj/17.11.2982.

Balakrishnan, R., J. Park, K. Karra, B.C. Hitz, G. Binkley, E.L. Hong, J. Sullivan, G. Micklem, and J.M. Cherry. 2012. YeastMine—an integrated data warehouse for Saccharomyces cerevisiae data as a multipurpose tool-kit. *Database*. 2012:bar062. doi:10.1093/database/bar062.

Banjade, S., L. Zhu, J.R. Jorgensen, S.W. Suzuki, and S.D. Emr. 2022. Recruitment and organization of ESCRT-0 and ubiquitinated cargo via condensation. *Sci Adv*. 8:eabm5149. doi:10.1126/sciadv.abm5149.

Best, J.T., P. Xu, J.G. McGuire, S.N. Leahy, and T.R. Graham. 2020. Yeast synaptobrevin, Snc1, engages distinct routes of postendocytic recycling mediated by a sorting nexin, Rcy1-COPI, and retromer. *Mol Biol Cell*. 31:944–962. doi:10.1091/mbc.e19-05-0290.

Buono, R.A., J. Paez-Valencia, N.D. Miller, K. Goodman, C. Spitzer, E.P. Spalding, and M.S. Otegui. 2016. Role of SKD1 Regulators LIP5 and IST1-LIKE1 in Endosomal Sorting and Plant Development. *Plant Physiol*. 171:251–264. doi:10.1104/pp.16.00240.

Cada, A.K., M.R. Pavlin, J.P. Castillo, A.B. Tong, K.P. Larsen, X. Ren, A. Yokom, F.-C. Tsai, J. Shiah, P.M. Bassereau, C.J. Bustamante, and J.H. Hurley. 2022. Reconstitution reveals friction-driven membrane scission by the human ESCRT-III proteins CHMP1B and IST1. *Biorxiv*. 2022.02.03.479062. doi:10.1101/2022.02.03.479062.

Chen, S.H., S. Chen, A.A. Tokarev, F. Liu, G. Jedd, and N. Segev. 2005. Ypt31/32 GTPases and their novel F-box effector protein Rcy1 regulate protein recycling. *Mol Biol Cell*. 16:178 192. doi:10.1091/mbc.e04-03-0258.

Chen, S.H., A.H. Shah, and N. Segev. 2014. Ypt31/32 GTPases and their F-Box effector Rcy1 regulate ubiquitination of recycling proteins. *Cell Logist*. 1:21 31. doi:10.4161/cl.1.1.14695.

Cherry, J.M., E.L. Hong, C. Amundsen, R. Balakrishnan, G. Binkley, E.T. Chan, K.R. Christie, M.C. Costanzo, S.S. Dwight, S.R. Engel, D.G. Fisk, J.E. Hirschman, B.C. Hitz, K. Karra, C.J. Krieger, S.R. Miyasato, R.S. Nash, J. Park, M.S. Skrzypek, M. Simison, S. Weng, and E.D. Wong. 2012. Saccharomyces Genome Database: the genomics resource of budding yeast. *Nucleic Acids Res*. 40:D700–D705. doi:10.1093/nar/gkr1029.

Crespo-Yàñez, X., C. Aguilar-Gurrieri, A.-C. Jacomin, A. Journet, M. Mortier, E. Taillebourg, E. Soleilhac, W. Weissenhorn, and M.-O. Fauvarque. 2018. CHMP1B is a target of USP8/UBPY regulated by ubiquitin during endocytosis. *Plos Genet*. 14:e1007456. doi:10.1371/journal.pgen.1007456.

Davis, N., J. Horecka, and G. Sprague. 1993. Cis- and trans-acting functions required for endocytosis of the yeast pheromone receptors. *J Cell Biology*. 122:53–65. doi:10.1083/jcb.122.1.53.

Day, K.J., J.C. Casler, and B.S. Glick. 2018. Budding Yeast Has a Minimal Endomembrane System. *Dev Cell*. 44:56 72.e4. doi:10.1016/j.devcel.2017.12.014.

Dimaano, C., C.B. Jones, A. Hanono, M. Curtiss, and M. Babst. 2008. Ist1 regulates Vps4 localization and assembly. *Mol Biol Cell*. 19:465 474. doi:10.1091/mbc.e07-08-0747.

Drury, G.E., A.A. Dowle, D.A. Ashford, W.M. Waterworth, J. Thomas, and C.E. West. 2012. Dynamics of plant histone modifications in response to DNA damage. *Biochem J*. 445:393–401. doi:10.1042/bj20111956.

Frankel, E.B., R. Shankar, J.J. Moresco, J.R. Yates, N. Volkmann, and A. Audhya. 2017. Ist1 regulates ESCRT-III assembly and function during multivesicular endosome biogenesis in Caenorhabditis elegans embryos. *Nat Commun*. 8:1439. doi:10.1038/s41467-017-01636-8.

Furuta, N., K. Fujimura-Kamada, K. Saito, T. Yamamoto, and K. Tanaka. 2007. Endocytic recycling in yeast is regulated by putative phospholipid translocases and the Ypt31p/32p-Rcy1p pathway. *Mol Biol Cell*. 18:295 312. doi:10.1091/mbc.e06-05-0461.

Galan, J.-M., A. Wiederkehr, J.H. Seol, R. Haguenauer-Tsapis, R.J. Deshaies, H. Riezman, and M. Peter. 2001. Skp1p and the F-Box Protein Rcy1p Form a Non-SCF Complex Involved in Recycling of the SNARE Snc1p in Yeast. *Mol Cell Biol*. 21:3105 3117. doi:10.1128/mcb.21.9.3105-3117.2001.

Goldenring, J.R. 2015. Recycling endosomes. *Curr Opin Cell Biol*. 35:117–122. doi:10.1016/j.ceb.2015.04.018.

Grant, B.D., and J.G. Donaldson. 2009. Pathways and mechanisms of endocytic recycling. *Nat Rev Mol Cell Bio*. 10:597 608. doi:10.1038/nrm2755.

Han, H., N. Monroe, W.I. Sundquist, P.S. Shen, and C.P. Hill. 2017. The AAA ATPase Vps4 binds ESCRT-III substrates through a repeating array of dipeptide-binding pockets. *Elife*. 6:e31324. doi:10.7554/elife.31324.

Hanamatsu, H., K. Fujimura-Kamada, T. Yamamoto, N. Furuta, and K. Tanaka. 2014. Interaction of the phospholipid flippase Drs2p with the F-box protein Rcy1p plays an important role in early endosome to trans-Golgi network vesicle transport in yeast. *J Biochem*. 155:51 62. doi:10.1093/jb/mvt094.

Hanson, P.I., R. Roth, Y. Lin, and J.E. Heuser. 2008. Plasma membrane deformation by circular arrays of ESCRT-III protein filaments. *J Cell Biology*. 180:389 402. doi:10.1083/jcb.200707031.

Hein, C., J. Springael, C. Volland, R. Haguenauer-Tsapis, and B. André. 1995. NPI1, an essential yeast gene involved in induced degradation of Gap1 and Fur4 permeases, encodes the Rsp5 ubiquitin—protein ligase. *Mol Microbiol*. 18:77–87. doi:10.1111/j.1365-2958.1995.mmi_18010077.x.

Hettema, E.H., M.J. Lewis, M.W. Black, and H.R.B. Pelham. 2003. Retromer and the sorting nexins Snx4/41/42 mediate distinct retrieval pathways from yeast endosomes. *Embo J*. 22:548 557. doi:10.1093/emboj/cdg062.

Hua, Z., P. Fatheddin, and T.R. Graham. 2002. An essential subfamily of Drs2p-related P-type ATPases is required for protein trafficking between Golgi complex and endosomal/vacuolar system. *Mol Biol Cell*. 13:3162 3177. doi:10.1091/mbc.e02-03-0172.

Isnard, A.-D., D. Thomas, and Y. Surdin-Kerjan. 1996. The Study of Methionine Uptake inSaccharomyces cerevisiaeReveals a New Family of Amino Acid Permeases. *J Mol Biol*. 262:473–484. doi:10.1006/jmbi.1996.0529.

Johnson, S.S., P.K. Hanson, R. Manoharlal, S.E. Brice, L.A. Cowart, and W.S. Moye-Rowley. 2010. Regulation of yeast nutrient permease endocytosis by ATP-binding cassette transporters and a seven-transmembrane protein, RSB1. *J Biol Chem*. 285:35792 35802. doi:10.1074/jbc.m110.162883.

Jones, C.B., E.M. Ott, J.M. Keener, M. Curtiss, V. Sandrin, and M. Babst. 2012. Regulation of Membrane Protein Degradation by Starvation-Response Pathways. *Traffic*. 13:468 482. doi:10.1111/j.1600-0854.2011.01314.x.

Katzmann, D.J., M. Babst, and S.D. Emr. 2001. Ubiquitin-Dependent Sorting into the Multivesicular Body Pathway Requires the Function of a Conserved Endosomal Protein Sorting Complex, ESCRT-I. *Cell*. 106:145 155. doi:10.1016/s0092-8674(01)00434-2.

Keener, J.M., and M. Babst. 2013. Quality Control and Substrate-Dependent Downregulation of the Nutrient Transporter Fur4. *Traffic*. 14:412 427. doi:10.1111/tra.12039.

Laidlaw, K.M.E., D.D. Bisinski, S. Shashkova, K.M. Paine, M.A. Veillon, M.C. Leake, and C. MacDonald. 2020. A glucose-starvation response governs endocytic trafficking and eisosomal retention of surface cargoes in budding yeast. *J Cell Sci*. 134:jcs257733. doi:10.1242/jcs.257733.

Laidlaw, K.M.E., and C. MacDonald. 2018. Endosomal trafficking of yeast membrane proteins. *Biochem Soc T*. 46:1551–1558. doi:10.1042/bst20180258.

Lewis, M.J., B.J. Nichols, C. Prescianotto-Baschong, H. Riezman, and H.R. Pelham. 2000. Specific retrieval of the exocytic SNARE Snc1p from early yeast endosomes. *Molecular biology of the cell*. 11:23 38.

Lin, C.H., J.A. MacGurn, T. Chu, C.J. Stefan, and S.D. Emr. 2008. Arrestin-Related Ubiquitin-Ligase Adaptors Regulate Endocytosis and Protein Turnover at the Cell Surface. *Cell*. 135:714 725. doi:10.1016/j.cell.2008.09.025.

Ma, M., and C.G. Burd. 2019. Retrograde trafficking and plasma membrane recycling pathways of the budding yeast Saccharomyces cerevisiae. *Traffic*. doi:10.1111/tra.12693.

Ma, M., C.G. Burd, and R.J. Chi. 2017. Distinct complexes of yeast Snx4 family SNX-BARs mediate retrograde trafficking of Snc1 and Atg27. *Traffic*. 18:134 144. doi:10.1111/tra.12462.

MacDonald, C., N.J. Buchkovich, D.K. Stringer, S.D. Emr, and R.C. Piper. 2012a. Cargo ubiquitination is essential for multivesicular body intralumenal vesicle formation. *Embo Rep*. 13:331 338. doi:10.1038/embor.2012.18.

MacDonald, C., J.A. Payne, M. Aboian, W. Smith, D.J. Katzmann, and R.C. Piper. 2015. A Family of Tetraspans Organizes Cargo for Sorting into Multivesicular Bodies. *Dev Cell*. 33:328 342. doi:10.1016/j.devcel.2015.03.007.

MacDonald, C., and R.C. Piper. 2015. Puromycin- and methotrexate-resistance cassettes and optimized Cre-recombinase expression plasmids for use in yeast. *Yeast*. 32:423 438. doi:10.1002/yea.3069.

MacDonald, C., and R.C. Piper. 2016. Cell surface recycling in yeast: mechanisms and machineries. *Biochem Soc T*. 44:474 478. doi:10.1042/bst20150263.

MacDonald, C., and R.C. Piper. 2017. Genetic dissection of early endosomal recycling highlights a TORC1-independent role for Rag GTPases. *J Cell Biol*. 8:jcb.201702177. doi:10.1083/jcb.201702177.

MacDonald, C., S.B. Shields, C.A. Williams, S. Winistorfer, and R.C. Piper. 2020. A Cycle of Ubiquitination Regulates Adaptor Function of the Nedd4-Family Ubiquitin Ligase Rsp5. *Curr Biology Cb*. doi:10.1016/j.cub.2019.11.086.

MacDonald, C., D.K. Stringer, and R.C. Piper. 2012b. Sna3 Is an Rsp5 Adaptor Protein that Relies on Ubiquitination for Its MVB Sorting. *Traffic*. 13:586 598. doi:10.1111/j.1600-0854.2011.01326.x.

MacDonald, C., S. Winistorfer, R.M. Pope, M.E. Wright, and R.C. Piper. 2017. Enzyme reversal to explore the function of yeast E3 ubiquitin-ligases. *Traffic*. 18:465 484. doi:10.1111/tra.12485.

Maity, S., C. Caillat, N. Miguet, G. Sulbaran, G. Effantin, G. Schoehn, W.H. Roos, and W. Weissenhorn. 2019. VPS4 triggers constriction and cleavage of ESCRT-III helical filaments. *Sci Adv*. 5:eaau7198. doi:10.1126/sciadv.aau7198.

McCullough, J., A.K. Clippinger, N. Talledge, M.L. Skowyra, M.G. Saunders, T.V. Naismith, L.A. Colf, P. Afonine, C. Arthur, W.I. Sundquist, P.I. Hanson, and A. Frost. 2015. Structure and membrane remodeling activity of ESCRT-III helical polymers. *Science*. 350:1548 1551. doi:10.1126/science.aad8305.

Menant, A., R. Barbey, and D. Thomas. 2006. Substrate-mediated remodeling of methionine transport by multiple ubiquitin-dependent mechanisms in yeast cells. *Embo J*. 25:4436–4447. doi:10.1038/sj.emboj.7601330.

Miura, K. 2020. Bleach correction ImageJ plugin for compensating the photobleaching of time-lapse sequences. *F1000research*. 9:1494. doi:10.12688/f1000research.27171.1.

Müller, M., O. Schmidt, M. Angelova, K. Faserl, S. Weys, L. Kremser, T. Pfaffenwimmer, T. Dalik, C. Kraft, Z. Trajanoski, H. Lindner, and D. Teis. 2015. The coordinated action of the MVB pathway and autophagy ensures cell survival during starvation. *Elife*. 4:e07736. doi:10.7554/elife.07736.

Nguyen, H.C., N. Talledge, J. McCullough, A. Sharma, F.R. Moss, J.H. Iwasa, M.D. Vershinin, W.I. Sundquist, and A. Frost. 2020. Membrane constriction and thinning by sequential ESCRT-III polymerization. *Nat Struct Mol Biol*. 27:392–399. doi:10.1038/s41594-020-0404-x.

Nickerson, D.P., M. West, and G. Odorizzi. 2006. Did2 coordinates Vps4-mediated dissociation of ESCRT-III from endosomes. *J Cell Biology*. 175:715 720. doi:10.1083/jcb.200606113.

O'Sullivan, M.J., and A.J. Lindsay. 2020. The Endosomal Recycling Pathway—At the Crossroads of the Cell. *Int J Mol Sci*. 21:6074. doi:10.3390/ijms21176074.

Paine, K.M., G.B. Ecclestone, and C. MacDonald. 2021. Fur4 mediated uracil-scavenging to screen for surface protein regulators. *Biorxiv*. 2021.05.27.445995. doi:10.1101/2021.05.27.445995.

Pfitzner, A.-K., V. Mercier, X. Jiang, J.M. von Filseck, B. Baum, A. Šarić, and A. Roux. 2020. An ESCRT-III Polymerization Sequence Drives Membrane Deformation and Fission. *Cell*. 182:1140-1155.e18. doi:10.1016/j.cell.2020.07.021.

Protopopov, V., B. Govindan, P. Novick, and J.E. Gerst. 1993. Homologs of the synaptobrevin/VAMP family of synaptic vesicle proteins function on the late secretory pathway in S. cerevisiae. *Cell*. 74:855–861. doi:10.1016/0092-8674(93)90465-3.

Rue, S.M., S. Mattei, S. Saksena, and S.D. Emr. 2008. Novel Ist1-Did2 complex functions at a late step in multivesicular body sorting. *Mol Biol Cell*. 19:475 484. doi:10.1091/mbc.e07-07-0694.

Saksena, S., J. Wahlman, D. Teis, A.E. Johnson, and S.D. Emr. 2009. Functional Reconstitution of ESCRT-III Assembly and Disassembly. *Cell*. 136:97 109. doi:10.1016/j.cell.2008.11.013.

Santos, R., O. Ursu, A. Gaulton, A.P. Bento, R.S. Donadi, C.G. Bologa, A. Karlsson, B. Al-Lazikani, A. Hersey, T.I. Oprea, and J.P. Overington. 2017. A comprehensive map of molecular drug targets. *Nat Rev Drug Discov*. 16:19–34. doi:10.1038/nrd.2016.230.

Sardana, R., and S.D. Emr. 2021. Membrane Protein Quality Control Mechanisms in the Endo-Lysosome System. *Trends Cell Biol*. doi:10.1016/j.tcb.2020.11.011.

Schothorst, J., H.N. Kankipati, M. Conrad, D.R. Samyn, G.V. Zeebroeck, Y. Popova, M. Rubio-Texeira, B.L. Persson, and J.M. Thevelein. 2013. Yeast nutrient transceptors provide novel insight in the functionality of membrane transporters. *Curr Genet*. 59:197–206. doi:10.1007/s00294-013-0413-y.

Seaman, M.N., J.M. McCaffery, and S.D. Emr. 1998. A membrane coat complex essential for endosome-to-Golgi retrograde transport in yeast. *The Journal of cell biology*. 142:665 681.

Séron, K., M.-O. Blondel, R. Haguenauer-Tsapis, and C. Volland. 1999. Uracil-Induced Down-Regulation of the Yeast Uracil Permease. *J Bacteriol*. 181:1793–1800. doi:10.1128/jb.181.6.1793-1800.1999.

Shestakova, A., A. Hanono, S. Drosner, M. Curtiss, B.A. Davies, D.J. Katzmann, and M. Babst. 2010. Assembly of the AAA ATPase Vps4 on ESCRT-III. *Mol Biol Cell*. 21:1059 1071. doi:10.1091/mbc.e09-07-0572.

Shi, Y., C.J. Stefan, S.M. Rue, D. Teis, and S.D. Emr. 2011. Two novel WD40 domain-containing proteins, Ere1 and Ere2, function in the retromer-mediated endosomal recycling pathway. *Mol Biol Cell*. 22:4093 4107. doi:10.1091/mbc.e11-05-0440.

Shields, S.B., A.J. Oestreich, S. Winistorfer, D. Nguyen, J.A. Payne, D.J. Katzmann, and R. Piper. 2009. ESCRT ubiquitin-binding domains function cooperatively during MVB cargo sorting. *J Cell Biology*. 185:213 224. doi:10.1083/jcb.200811130.

Sigismund, S., L. Lanzetti, G. Scita, and P.P.D. Fiore. 2021. Endocytosis in the context-dependent regulation of individual and collective cell properties. *Nat Rev Mol Cell Bio*. 22:625–643. doi:10.1038/s41580-021-00375-5.
Stalder, D., and D.C. Gershlick. 2020. Direct trafficking pathways from the Golgi apparatus to the plasma membrane. *Semin Cell Dev Biol*. 107:112–125. doi:10.1016/j.semcdb.2020.04.001.
Stringer, D.K., and R.C. Piper. 2011. A single ubiquitin is sufficient for cargo protein entry into MVBs in the absence of ESCRT ubiquitination. *J Cell Biology*. 192:229 242. doi:10.1083/jcb.201008121.
Swaney, D.L., C.D. Wenger, and J.J. Coon. 2010. Value of Using Multiple Proteases for Large-Scale Mass Spectrometry-Based Proteomics. *J Proteome Res*. 9:1323–1329. doi:10.1021/pr900863u.
Tan, J., B.A. Davies, J.A. Payne, L.M. Benson, and D.J. Katzmann. 2015. Conformational Changes in the Endosomal Sorting Complex Required for the Transport III Subunit Ist1 Lead to Distinct Modes of ATPase Vps4 Regulation. *J Biol Chem*. 290:30053 30065. doi:10.1074/jbc.m115.665604.
Tang, S., W.M. Henne, P.P. Borbat, N.J. Buchkovich, J.H. Freed, Y. Mao, J.C. Fromme, and S.D. Emr. 2015. Structural basis for activation, assembly and membrane binding of ESCRT-III Snf7 filaments. *Elife*. 4:e12548. doi:10.7554/elife.12548.
Thevenaz, P., U.E. Ruttimann, and M. Unser. 1998. A pyramid approach to subpixel registration based on intensity. *Ieee T Image Process*. 7:27–41. doi:10.1109/83.650848.
Urbanowski, J.L., and R.C. Piper. 2001. Ubiquitin Sorts Proteins into the Intralumenal Degradative Compartment of the Late-Endosome/Vacuole. *Traffic*. 2:622 630. doi:10.1034/j.1600-0854.2001.20905.x.
Valdez-Taubas, J., and H.R.B. Pelham. 2003. Slow Diffusion of Proteins in the Yeast Plasma Membrane Allows Polarity to Be Maintained by Endocytic Cycling. *Curr Biol*. 13:1636–1640. doi:10.1016/j.cub.2003.09.001.
Wang, B., S.L. Alam, H.H. Meyer, M. Payne, T.L. Stemmler, D.R. Davis, and W.I. Sundquist. 2003. Structure and Ubiquitin Interactions of the Conserved Zinc Finger Domain of Npl4*. *J Biol Chem*. 278:20225–20234. doi:10.1074/jbc.m300459200.
Wiederkehr, A., S. Avaro, C. Prescianotto-Baschong, R. Haguenauer-Tsapis, and H. Riezman. 2000. The F-Box Protein Rcy1p Is Involved in Endocytic Membrane Traffic and Recycling Out of an Early Endosome in Saccharomyces cerevisiae. *J Cell Biology*. 149:397–410. doi:10.1083/jcb.149.2.397.
Wollert, T., C. Wunder, J. Lippincott-Schwartz, and J.H. Hurley. 2009. Membrane scission by the ESCRT-III complex. *Nature*. 458:172 177. doi:10.1038/nature07836.
Xiao, J., X.-W. Chen, B.A. Davies, A.R. Saltiel, D.J. Katzmann, and Z. Xu. 2009. Structural basis of Ist1 function and Ist1-Did2 interaction in the multivesicular body pathway and cytokinesis. *Mol Biol Cell*. 20:3514 3524. doi:10.1091/mbc.e09-05-0403.
Xu, P., H.M. Hankins, C. MacDonald, S.J. Erlinger, M.N. Frazier, N.S. Diab, R.C. Piper, L.P. Jackson, J.A. MacGurn, and T.R. Graham. 2017. COPI mediates recycling of an exocytic SNARE by recognition of a ubiquitin sorting signal. *Elife*. 6:e28342. doi:10.7554/elife.28342.

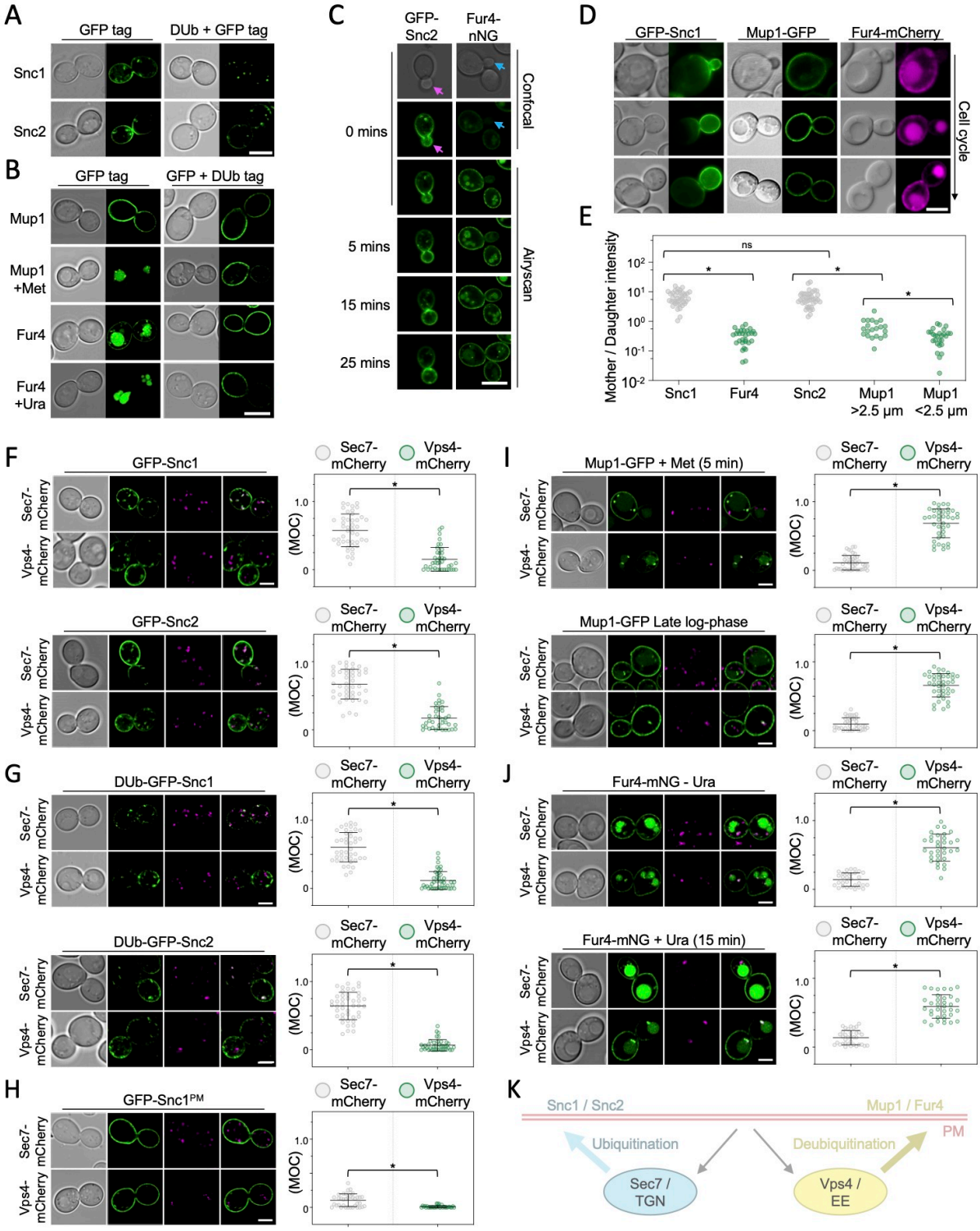

Figure 1: Differential trafficking features of recycling cargoes

A) Wild-type cells expressing Snc1 and Snc2 tagged with either GFP or a fusion of GFP with the catalytic domain of deubiquitinating enzyme UL36 (DUb + GFP) expressed from the *CUP1* promoter were imaged by Airyscan microscopy. **B)** Mup1 and Fur4 expressed from their endogenous promoters and fused to C-terminal GFP or GFP-DUb tags were imaged by Airyscan microscopy. Where indicated, 20 µg/ml methionine (+Met) and 40 µg/ml uracil (+Ura) was added to media 1-hour prior to imaging. **C)** Time-lapse microscopy of cells expressing GFP-Snc2 (left) or Fur4-mNG (right). **D-E)** Wild-type cells expressing fluorescently labelled Snc1, Mup1 and Fur4 were imaged, with example cell cycle stages depicted, and fluorescence in mother-daughter pairs quantified. * denotes $p < 0.002$. **F-J)** Indicated GFP tagged cargoes were imaged by Airyscan microscopy in Sec7-mCherry (upper micrographs) or Vps4-mCherry (lower micrographs) cells, with associated jitter plots of Mander's overlap coefficients (MOC). * denotes $p < 0.0001$ from unpaired *t*-test **K)** Schematic summarising distinct yeast endosomal recycling pathways. Scale bar, 5 µm.

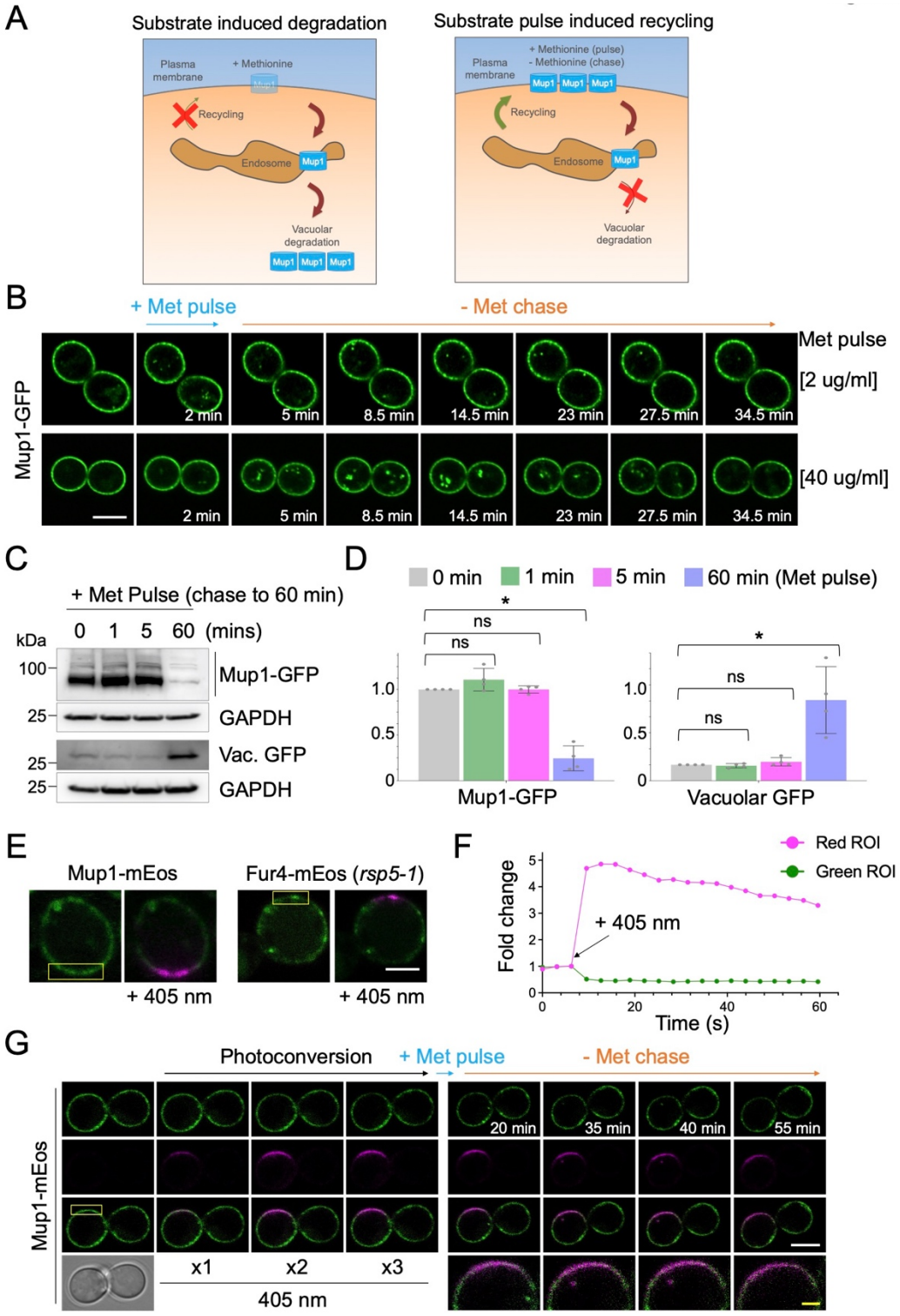

Figure 2: Substrate induced transporter recycling

A) Cartoon of substrate induced degradation (left) and recycling (right) of Mup1 triggered by modulation of extracellular methionine. **B)** Time-lapse Airyscan microscopy of cells expressing Mup1-GFP before and after 2-minute methionine (2 µg/ml, upper and 40 µg/ml, lower) pulse-chase incubations. **C)** Cells expressing Mup1-GFP were incubated with 20 µg/ml methionine for 0, 1, 5 and 60 mins followed by 3x washes and further incubation in SC-Met up to 60-minutes before lysates generated and immunoblotted. **D)** Quantification of average intensity of Mup1-GFP (left) and vacuolar processed GFP (right) from methionine pulse-chase experiments from **(C)**. * denotes $p < 0.01$. **E-F)** Yellow regions from cells expressing Mup1-mEos and Fur4-mEos were exposed to 405 nm laser at 0.5% to photoconvert molecules (left) and mEOS fluorescence tracked over time before (right). **G)** Time lapse microscopy of cells expressing Mup1-mEOS following 3x pulse with 0.1% 405 nm laser followed by substrate induced recycling stimulated by 2 µg/ml methionine for 30 seconds. Scale bar,5 µm (white); 1 µm (yellow).

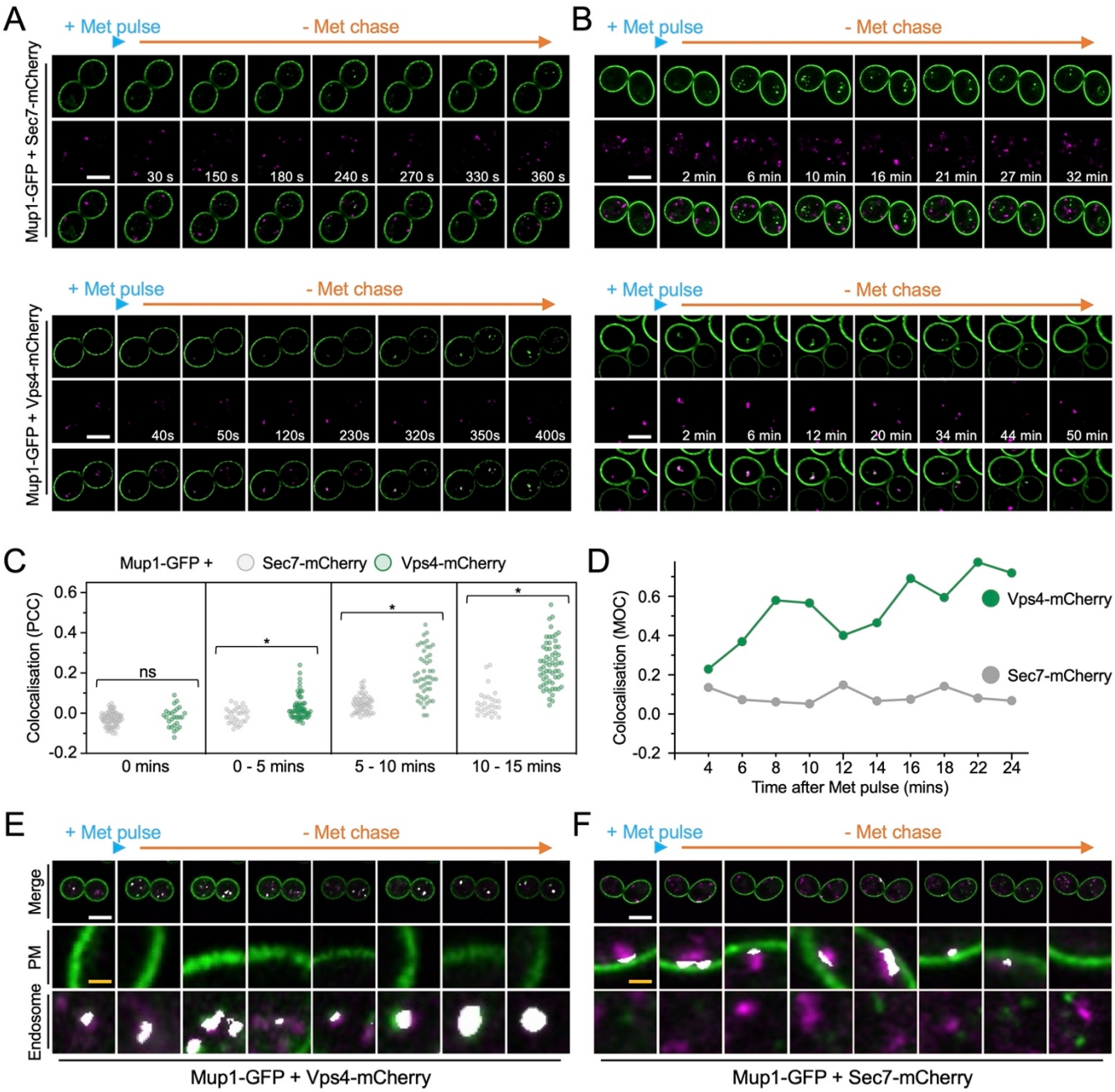

Figure 3: Mup1-GFP recycling occurs from a Vps4-Ist1 endosome

A-B) 4D Airyscan microscopy of wild-type cells co-expressing Mup1-GFP and Sec7-mCherry (upper) and Vps4-mCherry (lower) following a 30 second 20 µg/ml methionine pulse and subsequent SC-Met chase period over short 2-4s **(A)** and long 30-60s **(B)** imaging intervals. **C)** Quantification of Pearson's correlation coefficients between intercellular Mup1-GFP and either Sec7-mCherry (grey) or Vps4-mCherry (green) signal from steady state images acquired at indicated times during methionine pulse-chase (n = >27 cells), * represents $p < 0.002$ from Student's *t* test. **D)** Mander's overlap coefficient between Mup1-GFP and either Sec7-mCherry (grey) or Vps4-mCherry (green) from representative real-time methionine pulse chase imaging experiment. **E-F)** Time-lapse Airyscan micrographs of Mup1-GFP and Sec7-mCherry **(E)** or Vps4-mCherry **(F)** was analysed by Zen Black coloc software and regions of Manders overlap (not signal colocalization) above background that were detected are depicted in white, with zoomed in representations of the plasma membrane (PM) and endosome. Scale bar, 5 µm (white); 0.5 µm (yellow).

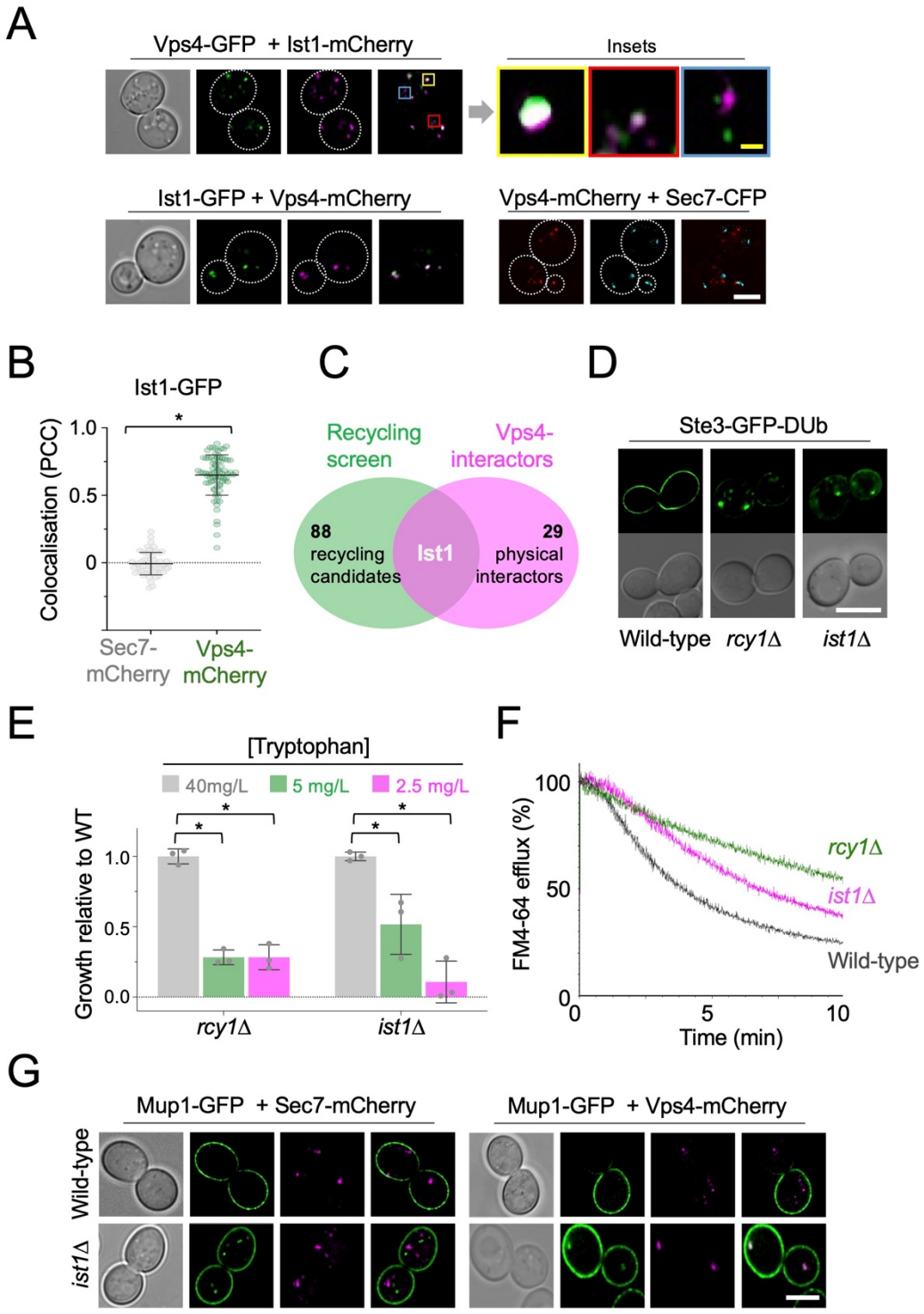

Figure 4: Ist1 is required for endosomal recycling in yeast

A) Wild-type cells co-expressing fluorescently labelled versions of Ist1, Vps4 and Sec7 were imaged by Airyscan microscopy. Insets show variation of colocalization. **B)** Pearson's correlation coefficient's calculated For Ist1-GFP with Sec7-mCherry (grey) and Vps4-mCherry (green). **C)** Venn diagram comparing 89 recycling factors (green) with known physical interactors of Vps4 (pink). **D)** Localization of stably integrated Ste3-GFP-DUb in indicated strains by Airyscan microscopy. **E)** Histogram showing relative growth of *rcy1*Δ and *ist1*Δ mutants compared with wild-type cells across media containing indicated concentrations of tryptophan. * represents $p < 0.02$ from unpaired *t*-test. **F)** FM4-64 efflux measurements from wild-type, *rcy1*Δ, and *ist1*Δ cells loaded with dye for 8 minutes at room temperature followed by 3x ice-cold media washes. **G)** Airyscan microscopy images of cells co-expressing Mup1-GFP and Sec7-mCherry (left) or Vps4-mCherry (right) in wild-type or *ist1*Δ cells. Scale bars, 5 µm (white); 0.5 µm (yellow).

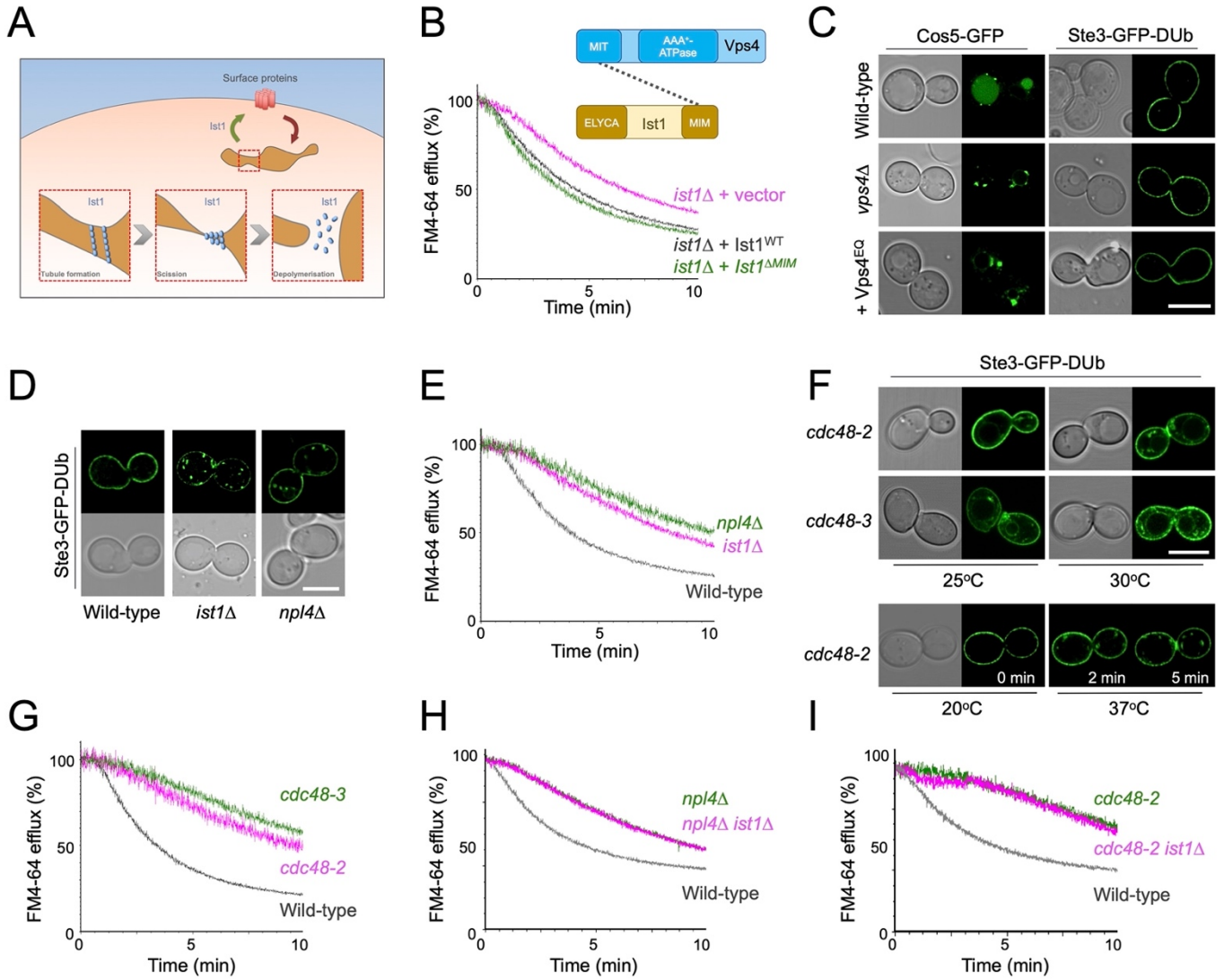

Figure 5: Npl4-Cdc48 implicated in Ist1-mediated recycling pathway

A) Schematic representation of model for how yeast Ist1 could drive recycling, based on studies on human IST1 that drives polymerisation / scission of endosome tubules to return material to the surface. **B)** Efflux measurements were recorded from *ist1*Δ cells transformed with either vector control or plasmids expressing Ist1^{WT} or Ist1$^{\Delta MIM}$ loaded with FM4-64 for 8 minutes at room temperature followed by ice cold washes. Cartoon representation of domain interaction between Vps4 and Ist1 included above. **C)** Airyscan confocal microscopy of Cos5-GFP from a plasmid (left) or stably integrated Ste3-GFP-DUb (right) expressed in wild-type and *vps4*Δ cells, and also in the presence of Vps4^{EQ} expressed from the *CUP1* promoter in the presence of 100 µM copper chloride. **D)** Stably integrated Ste3-GFP-DUb expressed in wild-type, *ist1*Δ, and *npl4*Δ cells imaged by Airyscan confocal microscopy. **E)** FM4-64 efflux measurements from indicated strains wild-type, *npl4*Δ, and *ist1*Δ cells grown to mid-log phase prior to loading with dye for 8 minutes at room temperature and efflux measured after washes. **F)** Stably integrated Ste3-GFP-DUb was expressed in strains habouring temperature sensitive alleles of *CDC48* (*cdc48-2* and *cdc48-3*), grown to mid-log phase at 25ºC, and imaged by Airyscan confocal microscopy directly or following a 30-minute incubation at 30ºC. **G-I)** Efflux measurements from indicated cells first loaded with FM4-64 for 8 minutes, washed 3x prior to cytometry. Scale bar, 5 µm.

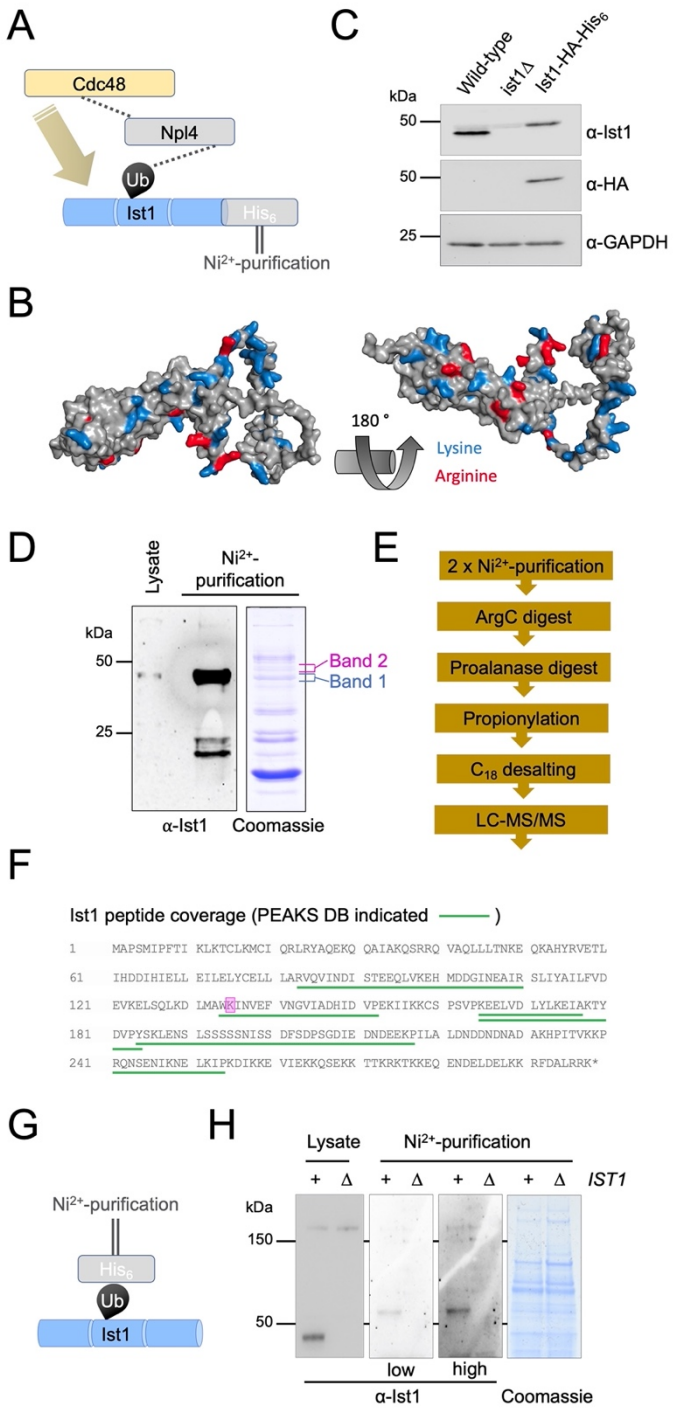

Figure 6: Ist1 is ubiquitinated in vivo

A) Simplified representation of known interactions (dotted lines) between Cdc48, Npl4 and Ubiquitin. We hypothesize this Npl4-Cdc48 enzyme module functionally connects with Ist1 via Ist1 ubiquitination. **B)** Alphafold structural model of yeast Ist1 with lysine (blue) and arginine (red) residues indicated. **C)** Immunoblot of lysates from wild-type, *ist1*Δ and Ist1-HA-His_6 strains using α-Ist1, α-HA and α-GAPDH antibodies. **D)** Whole cell lysates were generated from cells expressing Ist1-HA-His_6 and run on the same SDS-PAGE gel as 0.5% of the purified elution from 2 L culture followed by immunoblotting using α-Ist1 antibodies (left). A separate gel with 10% of purified sample was stained with Coomassie (right) and the bands excised for mass-spectrometry based identification indicated. **E)** Flow diagram depicting sequence of sample preparation for mass spectrometry analysis of Ist1 targeted at identifying ubiquitinated peptides. **F)** Ist1 amino acid sequence annotated with identified peptides (green) and potentially ubiquitinated lysine residue (pink) shown from PEAKS analysis. **G)** Simplified schematic of Ni^{2+}-NTA purification of the ubiquitome to test is Ist1 is ubiquitinated. **H)** Immunoblot using α-Ist1 antibodies of lysates generated from His_6-Ubiquitin with (+) or lacking (Δ) *IST1* (left). 2L from each of these cells was purified via Ni^{2+}-NTA twice and analysed by immunoblot and levels indicated by Coomassie staining (right).

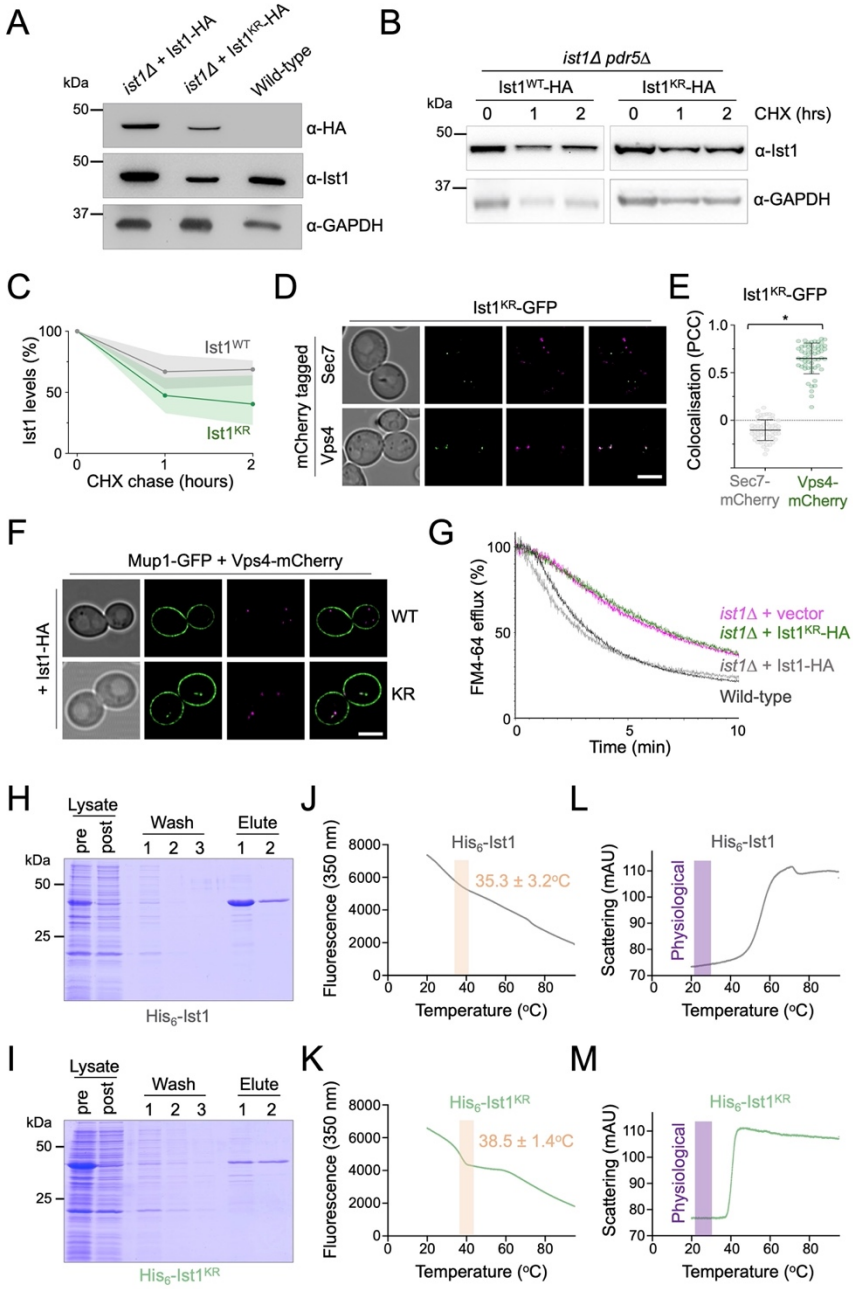

Figure 7: Lysineless Ist1 is defective in endosomal recycling

A) Immunoblot with indicated antibodies of lysates generated from *ist1*Δ cells transformed with plasmids expressing Ist1^{WT}-HA, or Ist1^{KR}-HA from endogenous promoter, alongside wild-type cells. **B)** Cycloheximide chase experiments using *ist1*Δ *pdr5*Δ cells expressing Ist1^{WT}-HA, or Ist1^{KR}-HA. Cells grown to mid-log phase were then exposed to 25 mg/L cycloheximide for the denoted time before harvesting and immunoblot with α-Ist1 and α-GAPDH antibodies. **C)** Graph of Ist1 stability following cycloheximide chase at indicated times of Ist1^{WT} (grey) and Ist1^{KR} (green), with standard deviation (n=3) indicated with respective shaded regions.
D) Airyscan images of *ist1*Δ cells co-expressing Ist1^{KR}-GFP and Sec7-mCherry (upper) or Vps4-mCherry (lower) grown to mid log phase. **E)** Associated jitter plots from (D) showing Pearson's correlation coefficient. * denotes $p < 0.0001$ from unpaired *t*-test. **E)** Airyscan microscopy of *ist1*Δ cells co-expressing Mup1-GFP, Vps4-mCherry with either Ist1^{WT}-HA (upper) or Ist1^{KR}-HA (lower). **F)** FM4-64 efflux measurements from wild-type cells (dark grey) and *ist1*Δ mutants expressing plasmid borne copies of Ist1^{WT}-HA (light grey), Ist1^{KR}-HA (green) or transformed with an empty vector (pink). **H-I)** Plasmids of His$_6$-Ist1^{WT} and His$_6$-Ist1^{KR} were expressed in BL21 DE3 codon optimized *E. coli* strain using 0.5 mM IPTG at 15ºC over-night. Lysates were generated by sonication and bound to 600µl Ni^{2+}-NTA bed volume, followed by washing in 20mM imidazole and elution in 500mM imidazole. Samples were analyzed by SDS-PAGE followed by Coomassie staining, showing protein levels in lysate pre- and post-binding to beads, the material lost during washes and the final eluted products. **J-M)** Intrinsic fluorescence at 350nm (J-K) and unfolding induced aggregation via scattering (L-M) was measured by nanoDSF for purified His$_6$-Ist1^{WT} and His$_6$-Ist1^{KR} samples exposed to a 1ºC / minute heat ramp**.** Scale bar, 5 µm.

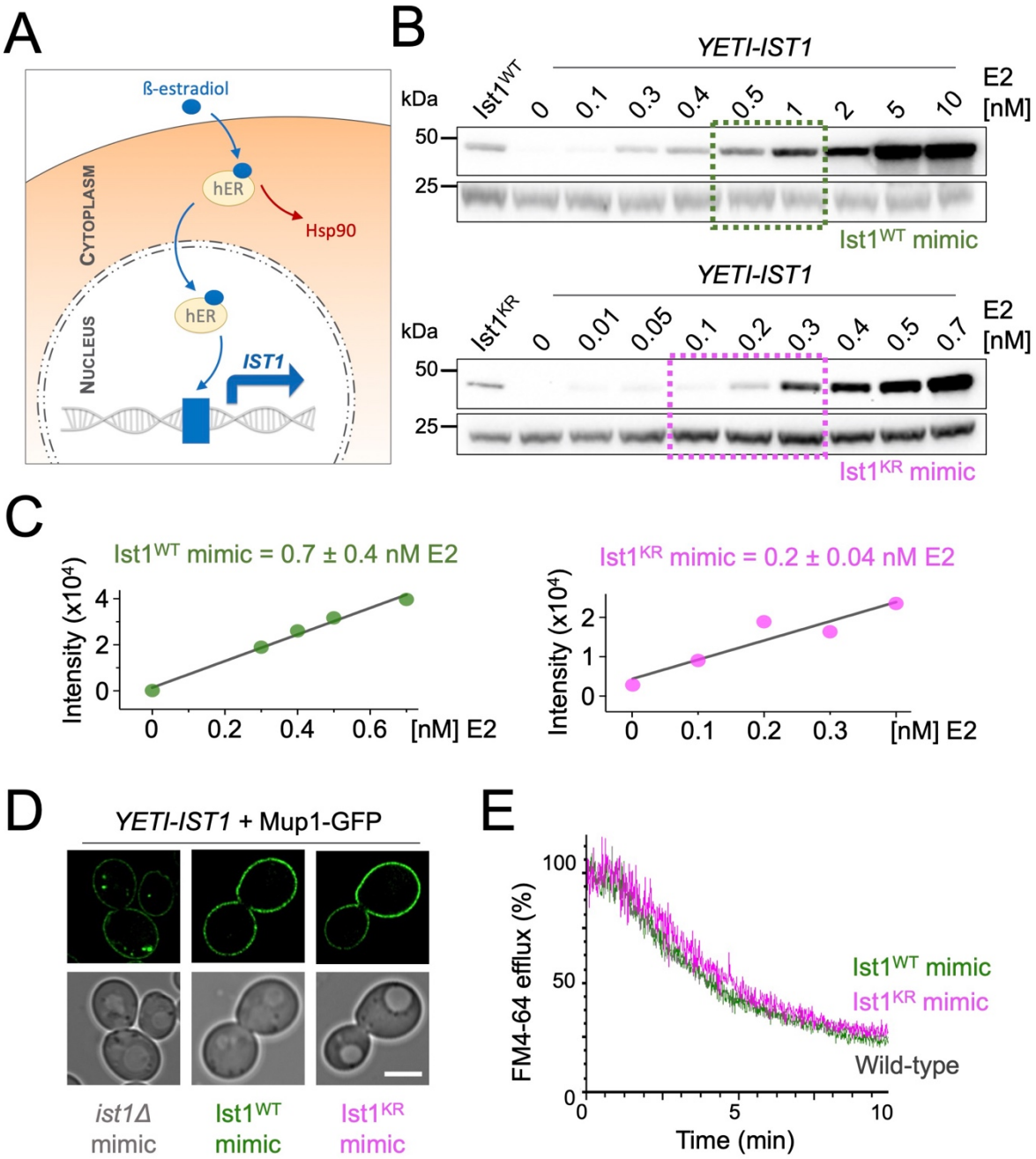

Figure 8: Reduced levels of ubiquitinatable Ist1 are sufficient for recycling
A) Schematic showing yeast estradiol titratable induction (YETI) system to regulate levels of *IST1* expression. **B-C)** Immunoblot depicting Ist1 levels from *YETI-IST1* cells exposed to indicated β-estradiol titrations with concentrations used to mimic $Ist1^{WT}$ (green) and $Ist1^{KR}$ (pink) levels estimated with standard deviation (n=3) shown. **D)** Airyscan microscopy of Mup1-GFP expressed in *YETI-IST1* cells exposed to β-estradiol concentrations required to mimic *ist1*Δ, $Ist1^{WT}$ and $Ist1^{KR}$ levels for 6 hours prior to imaging. **E)** FM4-64 efflux measurements from wild-type cells and *YETI-IST1* cells exposed to β-estradiol to mimic $Ist1^{WT}$ and $Ist1^{KR}$ levels prior to loading with dye for 8 minutes at room temperature. Scale bar, 5 µm.

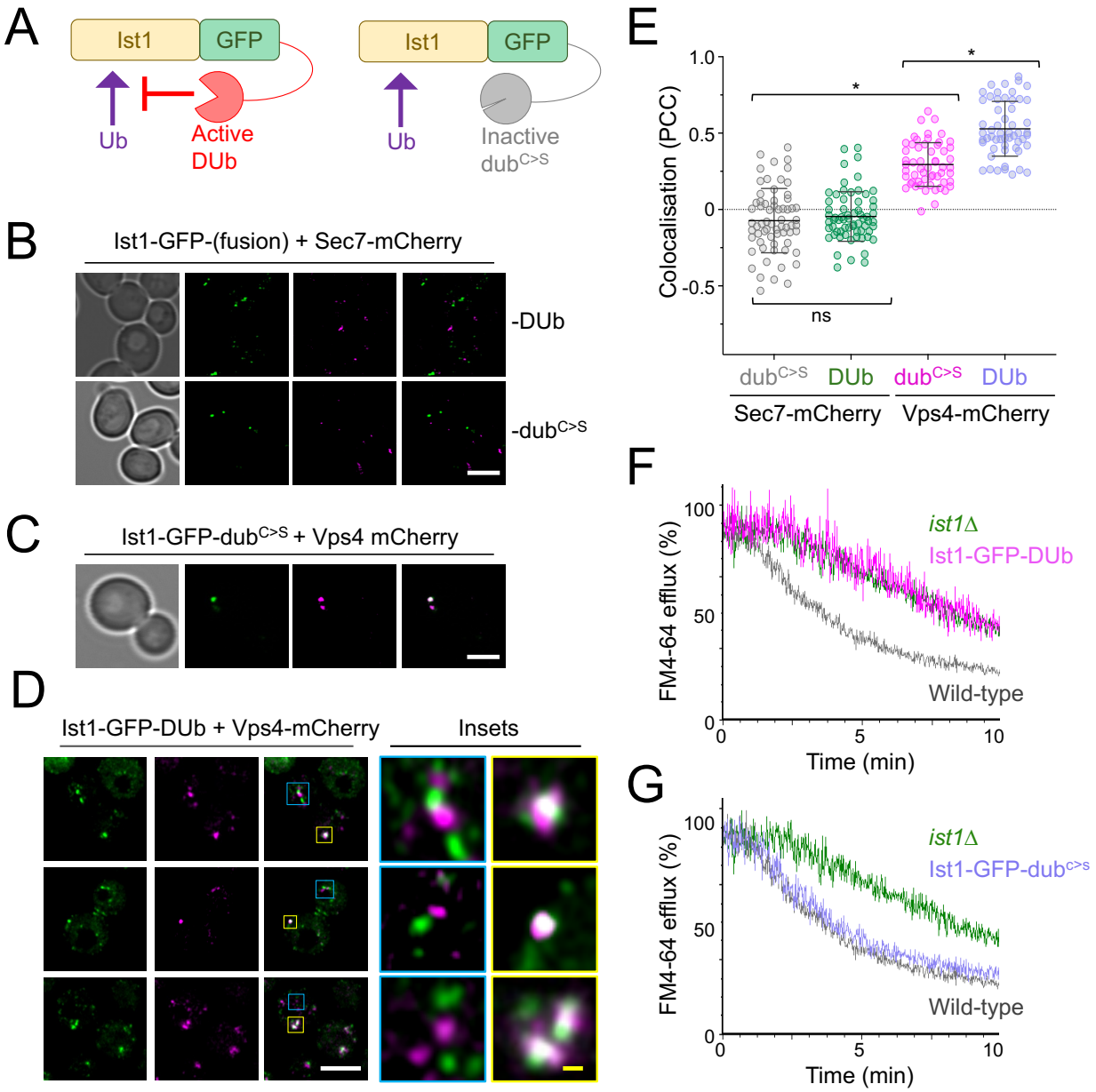

Figure 9: Reversal of Ist1 ubiquitination inhibits endosomal recycling

A) Schematic illustrating the strategy to fuse Ist1-GFP to an active deubiquitinating enzyme (DUb) and an inactive catalytically dead (dub$^{C>S}$) mutant enzyme. **B-D)** Airyscan microscopy of indicated fluorescent proteins expressed in wild-type cells grown to exponential phase prior to imaging. Insets (D) show of colocalization and distinct foci in yellow and blue, respectively. **E)** Jitter plots showing Pearson's correlation coefficient (PCC) from imaging shown in B-D. * denotes $p < 0.0001$ from unpaired *t*-test. **F-G)** FM4-64 efflux measurements from dye loaded to cells expressing active Ist1-GFP-DUb (F) and inactive Ist1-GFP- DUb$^{C>S}$ (G) fusion proteins, with profiles from wild-type and *ist1*Δ mutants included for reference. Scale bar, 5 µm (white); 0.5 µm (yellow).